Northern Hemisphere Sea Ice in KCM with and without Flux Correction

---

Bachelor Thesis

B. Sc. Physics of the Earth System - Meteorology, Oceanography, Geophysics

Faculty of Mathematics and Natural Sciences
Christian Albrechts University Kiel
GEOMAR Helmholtz Centre for Ocean Research Kiel

Author: **Philip Kreußler**
Matriculation number: **1018085**

First examiner: Prof. Dr. Mojib Latif
Second examiner: Dr. Thomas Martin

Kiel, 17th October 2016

Contents

Zusammenfassung

Korrekturen des oberflächennahen Salzgehalts im nordatlantischen Sektor des Kieler Klimamodells konnten markante systematische Fehler in mehreren Größen im Vergleich zu einem Kontrolllauf verringern. Vor allem die Verbesserung der Atlantic Meridional Overturning Circulation (AMOC) konnte zu einer Reduktion des Fehlers in der oberflächennahen Meerestemperatur führen. Im Gegenzug wurde die Simulation von arktischem Meereis verschlechtert. In dieser Arbeit wurde der Einfluss der Salzgehaltskorrektur auf arktisches Meereis, seine Variabilität sowie atmosphärische und ozeanische Parameter, die mit ihm in Verbindung stehen, untersucht. Um die Auswirkungen im Vergleich zu dem Kontrolllauf zu beurteilen, wurden Analysen des mittleren Zustands durchgeführt, Empirische Orthognal Funktionen angewandt und Korrelationen zwischen verschiedenen Größen realisiert. Dabei führt ein erhöhter Wärmetransport durch die AMOC zu einem Anstieg der oberflächennahen Lufttemperatur in den mittleren Breiten des Atlantiks und in der Labrador See. Eine Zunahme der Meereiskonzentration in der Grönland See wird durch eine flächenmäßig größere Abnahme in der Labrador See maskiert, sodass es zu einer Gesamtabnahme des Meereises kommt. Beide Läufe sind durch einen rasanten Regimewechsel in der Fläche des Meereises charakterisiert, der durch eine drastische Verringerung des Einstroms von Wasser und dem damit verbundenen Wärmetransport in die Barents See hervorgerufen wird. Dieser Regimewechsel wird durch eine positive Rückkopplung mit oberflächennahen Westwinden aufrecht erhalten. Im Gegensatz zum Kontrolllauf besteht eine verbesserte Fähigkeit, den Kipppunkt für den Regimewechsel in den Ausgangszustand zu überschreiten. Des Weiteren wird die Variabilität des Meereises durch die Störung des Wärmeeinstroms in beiden Läufen beeinflusst. Neben dem Einstromevent kann die Nordatlantische Oszillation als treibende Kraft für die Meereisvariabilität ausgemacht werden und damit Beobachtungen bestätigen. Aufgrund des massiven Eisverlustes in der Labrador See ist der korrigierte Lauf nicht in der Lage, beobachtete Muster dort widerzuspiegeln. Die Salzgehaltskorrektur kann zwar zu einer realistischeren Wiedergabe von vielen Parametern beitragen, die Simulation von Meereis und dessen Variabilität bleibt jedoch ein großes Problem im Kieler Klimamodell. Für zukünftige Experimente mit dem Kieler Klimamodell sollten die Fehler bezüglich der Darstellung von arktischem Meereis weiter verbessert werden.

Abstract

Performed sea surface salinity (SSS) corrections in the North Atlantic sector of the Kiel Climate Model yielded an alleviation of prominent biases relative to a control run. Especially an enhanced representation of the Atlantic Meridional Overturning Circulation (AMOC) could improve the bias in sea surface temperature in the corrected run. In turn, the simulation of Arctic sea ice was degraded. This study examines the impact of the SSS correction on Arctic sea ice, its variability and atmospheric and oceanic parameters influencing the former. Mean state and Empirical Orthogonal Function analyses as well as correlations were carried out in order to assess the leverage relative to the control run. It is found that the increased heat transport due to an enhanced AMOC results in a rise of surface air temperature in the mid-latitude Atlantic and the Labrador Sea. A gain in sea ice concentration (SIC) in the Greenland Sea is masked by a more extensive loss of sea ice in the Labrador Sea such that a total net loss of sea ice is stated. Both integrations inhibit a rapid climate transition in sea ice area, caused by a Barents Sea Inflow shutdown that is sustained by a positive feedback between the perturbation of heat inflow into the Barents Sea and surface near westerly winds. Relative to the control run an enhanced ability of tipping back to initial conditions is found. Moreover, SIC variability is affected by the mentioned regime shift in both integrations. Aside the shutdown event, the North Atlantic Oscillation is found as one of the major drivers for SIC variability which compares well to observations. Throughout the investigations, the corrected run fails to represent observed characteristics of the Labrador Sea due to the massive sea ice loss there. The SSS correction leads to a more realistic representation of many parameters but the simulation of sea ice and its variability remains an issue in the Kiel Climate Model. For future experiments the performance of the Kiel Climate Model has to be further improved regarding Arctic sea ice.

List of Abbreviations

AMOC Atlantic Meridional Overturning Circulation

AO Arctic Oscillation

BO Barents Oscillation

BS Barents Sea

BSI Barents Sea Inflow

CTL Control run

EOF Empirical Orthogonal Function

FWC Freshwater flux-corrected run

GS Greenland Sea

KCM Kiel Climate Model

LS Labrador Sea

PC Principal component

RBO Reversed Barents Oscillation

SAT Surface air temperature

SIA Sea ice area

SIC Sea ice concentration

SLP Sea level pressure

SSS Sea surface salinity

SST Sea surface temperature

STD Standard deviation

UVEL Zonal component of the surface ocean current

1 Introduction

Arctic sea ice decline has accelerated in recent years (*Kwok et al.*, 2009). It was found that internal variabilities make for as much as up to 50 % of the total sea ice loss (*Stroeve, Holland et al.*, 2007). This is one reason for its own to maximise effort to gain as much knowledge as possible about internal variabilities. Another reason is the matter of fact that external forcings can easily be masked by internal variabilities such that their impacts remain unseen. To forestall such problems an excellent understanding of internal variability is needed.

The Kiel Climate Model (KCM) has been used to examine these variabilities but overestimates sea ice concentration (SIC) in the Arctic relative to observations. Like other climate models, KCM's representation of processes in the North Atlantic is relatively poor (*Flato et al.*, 2013; *Wang et al.*, 2014), for instance there's a significant cold bias in sea surface temperature (SST) that consequently favours the formation of sea ice (*Drews et al.*, 2015). Further, KCM inhibits a bias in the placement of the Gulf Stream and the North Atlantic Current. The path of the North Atlantic Current is too zonal and misses out on carrying heat into important regions in higher latitudes as the northwest corner in the east of Newfoundland (*Lazier*, 1994). In order to assess the question if too coarse model resolution is responsible for the SST bias, *Delworth, Rosati et al.* (2012) used a high-resolution model but found similar biases. Another suspect for causing the SST bias is salinity. *Reintges et al.* (2016) found that the representation of mean salinity is one of the major problems in climate models. Especially the North Atlantic and the Arctic feature too low salinities. This leads to an increased stratification and a diminished convection which also yields excessive sea ice, especially in the Labrador Sea. In addition, the Atlantic Meridional Overturning Circulation (AMOC) - an important mechanism for northward heat transport - is largely influenced by the salinity bias. Too low a density in the sinking regions tends to weaken the AMOC which in turn carries less heat into the sub-polar North Atlantic (*T. Park et al.*, 2016). In order to investigate if a more realistic representation of sea surface salinity (SSS) could alleviate the model's biases, *T. Park et al.* (2016) performed a freshwater flux correction. A clear improvement of the AMOC and the SST bias relative to a control run was achieved such that the sea ice concentration was reduced by around 40 % in the Labrador Sea. On the other side, the positive sea ice bias was enhanced in the Barents Sea. The representation of Arctic sea ice remains a problem in KCM (*T. Park et al.*, 2016) that isn't solely solved by correcting SSS due to the amount of parameters influencing sea ice.

Sea ice is a complex component of the cryosphere that interacts with various different processes from the atmosphere and ocean, for example the North Atlantic Oscillation (NAO). The NAO is the leading (wintertime) pattern of sea level pressure variability of the North Atlantic sector. *Fang et al.* (1994) and *Deser et al.* (2000) found the NAO

responsible for the largest portion of sea ice concentration variability in the Arctic sector of the Atlantic. The NAO is characterised by a strong dipole in the pressure field that has its out-of-phase centres of actions over the Azores and Iceland (*Hurrell*, 1995). The NAO's positive phase has it that anomalous high pressure over the Azores permits increased west winds to transport heat to the Eurasian continent which in turn yields higher-than-normal surface air temperatures (SAT) in this region and lower-than-normal temperatures over the Labrador Sea (*Hurrell*, 1996).

In a recent study, *Aue* (2016) found the Arctic Oscillation (AO) to be the atmospheric driver of the second mode of winter SIC variability. The AO or Northern Hemisphere annular mode is the leading (wintertime) atmospheric pattern of the entire Northern Hemisphere (*Thompson et al.*, 1998). *Thompson et al.* (1998) characterised it as the surface signature of modulations in the strength of the polar vortex aloft. The pressure field yields a strong dipole between the central Arctic and the surrounding zonal ring at 45°N with in-phase centres of action over the Azores and the Aleutian Islands (*Wallace et al.*, 2002). Similar to the NAO, positive AO phases have it that intensified west winds bring heat and thus increased SAT to the Eurasian continent with a more zonally distinct impact than the NAO (*Thompson et al.*, 1998). As a consequence, anomalous cold temperatures are observed over the Labrador Sea and the northeastern part of Canada (*Thompson et al.*, 1998).

Sea ice is not only influenced by atmospheric phenomena but it can affect them itself in return. Due to the shrinking of Arctic sea ice (*Vaughan et al.*, 2013), SIC plays a stronger role in affecting the climate system. For instance, a loss in sea ice modifies the oceanic albedo (*Stroeve, Serreze et al.*, 2012) and the heat flux between the ocean and the atmosphere such that surface air temperatures rise (*Petrie et al.*, 2015). *Pedersen et al.* (2016) concluded that this yields a decrease in the meridional temperature gradient and consequently in the thermal wind. *Francis et al.* (2012) suggested that a weakened thermal wind could possibly lead to a more persistent weather in Europe. Furher, impacts on the NAO were confirmed by *Deser et al.* (2000), *Bader et al.* (2011) and *Vihma* (2014).

The sea ice concentration can also be impacted by the ocean. Higher sea surface temperatures lead to a reduction of sea ice (*Mahajan et al.*, 2011). *Delworth & Mann* (2000) and *Polyakov et al.* (2010) found SST and SIC being influenced by the AMOC which is thought to be a major source of (multi-)decadal climate variability. The AMOC is a north-to-south conveyor belt for water masses that transports cool water from the North Atlantic to the south. On top, relatively warm water compared to the water below is taken to the north and thus net heat is brought to the North Atlantic. The AMOC is largely influenced by density gradients and prevailing convectional conditions.

The subject of this work is to assess the question what the mean state and the Arctic sea ice and its variability are like in the control run of KCM. Further, it is investigated

in what way the SSS correction affects oceanic and atmospheric parameters like AMOC and NAO and especially their implications on Arctic sea ice and its variability. In order to do this, EOF analyses for the North Atlantic are carried out for two integrations of KCM, a control run and a freshwater flux-corrected run. The paper is organised as follows: Sect. 2 provides the data used and the applied methods for analyses. In Sect. 3 the results of both integrations are assessed and discussed in Sect. 4.

2 Data and methods

The data used throughout this study derives from the Kiel Climate Model (KCM) that is described in Sect. 2.1. 5000 years of model data are available of which only 700 years are used for analyses. Two integrations, one with and the other without freshwater flux correction, are compared by assessing different atmospheric and oceanographic parameters. Further, definitions and used statistical analyses are explained in the following sections.

2.1 Kiel Climate Modell

KCM implements an atmospheric general circulation model which is coupled to a combined ocean-sea ice general circulation model (*W. Park et al.*, 2009). The atmospheric model used is ECHAM5[1] (*Roeckner et al.*, 2003) with a horizontal resolution of T42 ($2.8° \times 2.8°$) and 19 vertical levels (*T. Park et al.*, 2016). Coupled to ECHAM5 is the ocean-sea ice model NEMO[2], consisting of the ocean general circulation model OPA9[3] and the sea ice-snow model LIM2[4] (*Madec*, 2015). The ocean's resolution is with 31 levels in the vertical and with 2° in the horizontal. An enhanced meridional resolution of 0.5° close to the equator yields an average resolution of 1.3° (*W. Park et al.*, 2009). To connect both - the atmospheric and oceanic component - the OASIS3[5] coupler is employed (*Valcke*, 2013) that transfers and interpolates the data between the different grids described above (*W. Park et al.*, 2009).

2.1.1 Experiments

Two integrations of KCM are used for analyses. The control run (referred to as CTL throughout this work) doesn't use any form of flux correction or anomaly coupling for either freshwater, heat or wind stress (*W. Park et al.*, 2009; *Yeh et al.*, 2011). CTL is a pre-industrial run starting from Levitus[6] climatology and employing a CO_2-concentration of 286 ppm (*T. Park et al.*, 2016).

In order to reduce the large sea surface salinity bias in the North Atlantic, a freshwater flux correction was applied to CTL by *T. Park et al.* (2016). In a 100-year long run with Levitus climatology SSSs were restored to initial conditions monthly. From the last 50 years the resulting surface freshwater fluxes were calculated and added to the pre-industrial integration and yielded thefreshwater-corrected run (called FWC in

[1] Atmospheric general circulation model version 5
[2] Nucleus for European Modeling of the Ocean
[3] Océan Parallélisé version 9
[4] Louvain-la-Neuve Ice Model version 2
[5] Ocean Atmosphere Sea Ice Soil version 3
[6] National Oceanographic Data Center World Ocean Atlas 1994

the subsequent sections). For the spatial pattern of the annual-mean freshwater flux correction see figure 1 in *T. Park et al.* (2016). In total, the ocean gains freshwater of about 0.15 Sv, leading to a freshening of the ocean. As a consequence of the water input, sea surface height had to be reduced every year to conserve the global volume of water. Volume-mean salinities in the North Atlantic region required an adjustment time of at least 200 years to equilibrate from an initial drift which is why model years 1300-1999 are used for analyses in both integrations (*T. Park et al.*, 2016).

2.1.2 Data used for analyses

Both integrations are compared by studying the following parameters: sea ice concentration (SIC), sea level pressure (SLP), surface air temperature (SAT), Atlantic Meridional Overturning Circulation (AMOC) as well as the zonal component of the surface ocean current (UVEL). With a view to a slightly more handy quantity one auxiliary parameter is introduced in addition to these 5 parameters: sea ice area (SIA). SIA is calculated by multiplying SIC with the size of the corresponding grid cell, with $L = W = 2\pi r \cdot \frac{res}{360°}$, the length and the width of the cell in km and $res = 2.8°$, the model resolution:

$$SIA = SIC \cdot L \cdot W \cdot cos\,\phi = SIC \cdot \left(2\pi r \cdot \frac{res}{360°}\right)^2 \cdot cos\,\phi$$

whereas $r = 6371\ km$, the radius of the Earth, and ϕ, the geographical latitude in degrees. In order to investigate the interannual variability and thus to remove the annual cycle, only winter mean data for months from December through to March is analysed.

2.2 Definitions

The studied area of the North Atlantic is between 90°W−90°E and 30°N−90°N (and where data is available). Analyses of the Arctic start at 50°N and extend to the pole. Further examined areas are the Labrador Sea (LS) in the region from 60°W−45°W and 55°N−60°N, the Greenland Sea (GS) that ranges from 20°W−3°E and 64°N−80°N and the western part of the Barents Sea (BS) that extends from 3°E−43°E and 71°N−80°N.

To quantify the strength of the NAO, a NAO index in form of a normalised difference in pressure (p) anomalies between Lisbon (L) at 9°W, 39°N and Reykjavik (R) at 21°W, 24°N is used:

$$NAO = \frac{p_L(t) - \bar{p}_L}{\sigma_{p_L}} - \frac{p_R(t) - \bar{p}_R}{\sigma_{p_R}}$$

Further, to represent the strength of the AMOC, an AMOC index is defined as the maximum of the overturning streamfunction at 30°N.

2.3 Statistical methods

2.3.1 Mean and standard deviation

Throughout this study the mean of a value x is calculated by the following equation:

$$\bar{x} = \frac{1}{N} \sum_{i=1}^{N} x_i$$

with N the total number of samples and i the index number of the current sample. Another quantity used in statistics is the standard deviation (STD) σ. It describes the (statistical) spread of a value around its mean and can be a decent indicator for variability:

$$\sigma = \sqrt{\frac{1}{N-1} \sum_{i=1}^{N} (x_i - \bar{x})^2}$$

2.3.2 Correlation

A correlation examines the linear relationship between two time series x and y. Scaling the covariance Cov of two datasets by the product of their STDs σ, yields the correlation coefficient r_{xy} which in turn is a more handy measure for the relationship. The closer r_{xy} is to 1, the better is the positive connection, the closer r_{xy} is to -1, the better is the negative connection. A correlation coefficient of 0 means that there is no (linear) relationship at all. The explained variance is given by r_{xy}^2. In the following, $\mathcal{E}$ is the expected value of the considered quantity:

$$Cov(x, y) = \mathcal{E}[(x - \mathcal{E}(x)) \cdot (y - \mathcal{E}(y))]$$

$$r_{xy} = \frac{Cov(x, y)}{\sigma_x \sigma_y}$$

2.3.3 Linear regression and linear trend

Sometimes it is inevitable that data is detrended from its linear trend, for instance when examining internal variability. For this purpose a linear regression - the best fit linear function between N data points of two variables (x_i, y_i) in a least-squares error approach (*von Storch et al.*, 1999) - is made:

$$y_i = \alpha + \beta x_i$$

where α and β are the regression coefficients (intercept and slope). To eliminate the linear trend, this function is removed from the considered data. In the following, the term linear trend refers to the coefficient β.

2.3.4 Empirical Orthogonal Function

This section follows the description for Empirical Orthogonal Functions (EOFs) by *von Storch et al.* (1999) and *Jolliffe* (2002). EOF is a multivariate eigen technique that puts local variances of time series data into spatial relation, i.e. EOF makes simultaneous amplitudes of statistical variance at a given time visible. This allows to compare the variances' phases. Furthermore, it can not only provide one pre-dominant pattern (also called mode) but also less dominant patterns. At least, EOF enables time series of those described patterns by calculating a time depending coefficient, known as principal component (PC). The resulting patterns are by definition orthogonal to each other such that a physical interpretation of less dominant modes becomes difficult.

First of all to calculate the eigenvectors (patterns) $\vec{e}_i$ and corresponding PCs $\alpha_{i,t}$, the data of a m-dimensional random vector $\vec{X}_t$, observed at time t, has to be transformed so that it is an anomaly regarding the mean in time $\vec{\mu} = \mathcal{E}(\vec{X}_t)$:

$$\vec{X}'_t = \vec{X}_t - \vec{\mu}$$

It is the main purpose to expand these anomalies into a finite series

$$\vec{X}'_t = \sum_{i=1}^{k} \alpha_{i,t} \vec{e}_i$$

by projecting that m-dimensional random vector $\vec{X}'_t$ onto orthogonal, one-dimensional subspace spanning eigenvectors $\vec{e}_i$. This projection[7] produces the (dimensionless) PC $\alpha_{i,t} = \langle \vec{X}'_t, \vec{e}_i \rangle$ and breaks up the total variance onto those m different eigenvectors. There can't be more than $k = m$ eigenvectors, which moreover is the only case of equality. Using $k = m$ eigenvectors can consume lots of time for computing so that $k \ll m$ often is enough, also, because the significance of the least dominant patterns decreases rapidly. Having less than m patterns means in turn, that equality isn't given and that there is an error ϵ_i to $\vec{X}'_t$. If ϵ_i is minimised the variance of $\vec{X}_t$ regarding $\vec{e}_i$ is

[7] $\langle \cdot, \cdot \rangle$ denotes the inner product

maximised, the projection of the anomalies $\vec{X}'_t$ yields the optimal coefficient $\alpha_{i,t}$ and the patterns are specified:

$$\epsilon_i = \sum_t (\vec{X}'_t - \sum_{i=1}^{k} \alpha_{i,t}\vec{e}_i)^2 = \sum_t (\vec{X}'_t - \sum_{i=1}^{k} \langle \vec{X}'_t, \vec{e}_i \rangle \cdot \vec{e}_i)^2$$

Now, again by minimising the error under the constraint $\|\vec{e}_i\| = 1$, the eigenvectors can be calculated. The larger the index i gets, the longer is the expression for the error ϵ_i[8]:

$$\epsilon_1 = \mathcal{E}(\|\vec{X}'_t - \langle \vec{X}'_t, \vec{e}_1 \rangle \cdot \vec{e}_1\|^2)$$

$$\epsilon_2 = \mathcal{E}(\|\vec{X}'_t - \langle \vec{X}'_t, \vec{e}_1 \rangle \cdot \vec{e}_1 - \langle \vec{X}'_t, \vec{e}_2 \rangle \cdot \vec{e}_2\|^2)$$

The higher-order eigenvectors correspond to that approach. Mathematically spoken, this method is nothing but an axis transformation and calculating the coinciding covariance matrix. Every eigenvector $\vec{e}_i$ of this matrix is associated with an eigenvalue λ_i. This value is the pattern's explained proportion of the total variance $\sum_{i=1}^{m} \lambda_i$ that was broken up into m fractions when projecting $\vec{X}'_t$ onto the eigenvectors:

$$Var(\vec{e}_i) = \frac{\lambda_i}{\sum_{i=1}^{m} \lambda_i}$$

The pattern with the highest explained variance is called leading mode of the EOF or simply leading EOF.

[8] $\|\cdot\|$ denotes the vector norm

3 Results

In order to make the impacts of the SSS correction visible, as well in atmospheric features as in oceanic ones, the mean state and trend of both integrations are compared. Furthermore, the variability is examined by performing EOF analyses for different time periods of the integrations and connected to observations. SIA analyses and correlations of different parameters are carried out to quantify the influence of the SSS correction on the climate system.

3.1 Mean state

First of all, the leading two statistical moments of SIC, in form of mean and STD, are assessed. In comparison with observations KCM has excessive sea ice in the Atlantic sector of the Arctic. In CTL the Labrador Sea is partly covered by sea ice while the Barents Sea is entirely covered (Fig. 1a). In FWC an improvement of the mean sea ice concentration is found (Fig. 1b, c). A loss of up to 33 % in the LS is stated. This coincides with the findings of *T. Park et al.* (2016) who discovered a sea ice loss of up to 40 % in the LS. On the other hand, the Greenland Sea gains sea ice in total which is a degradation relative to CTL. The increase of almost 50 % is masked by the more extensive loss of sea ice in the LS such that the total SIA of the Atlantic sector of the Arctic reduces from $6.5 \cdot 10^6\ km^2$ to $6.3 \cdot 10^6\ km^2$. The Barents Sea shows a small decrease in mean SIC such that the suggested enhancement of the positive SIC bias in the BS found by *T. Park et al.* (2016) isn't confirmed here.

The maximums of SIC variability are close to the sea ice edge (Fig. 1d, e). The changes in SIC come along with a change in variability (Fig. 1c, f). The reduction in SIC in the LS yields a decreased SIC variability south of Greenland and an increased variability in the region southwest of Greenland which is indicative of a retreat of the sea ice edge in this region. The opposite can be seen in the GS where an enhanced mean SIC leads to a shift of the sea ice edge to the east where it almost enters the BS. Positive values of STD show the region in which the winter sea ice edge could possibly be located. The BS shows a weak negative signal in mean SIC accompanied by a slightly enhanced variability for the reasons stated above.

Local linear trend analyses for SIC show similar patterns for both integrations (Fig. 2a, b). Relative to CTL the amplitudes of the local trends in FWC are not as high which is an improvement for a climate model's stability. The SIC's trends in the LS and the GS are negative whereas the BS shows a positive trend in SIC. At first sight, this analysis doesn't support the finding of shrinking SIC in FWC because the trend in SIC rises in the LS. It should be minded that a rising trend hasn't to be due to a net gain in sea ice, it could also be due to a slower rate of SIC loss. An increased trend of 0.07 $\frac{\%}{year}$ in SIC

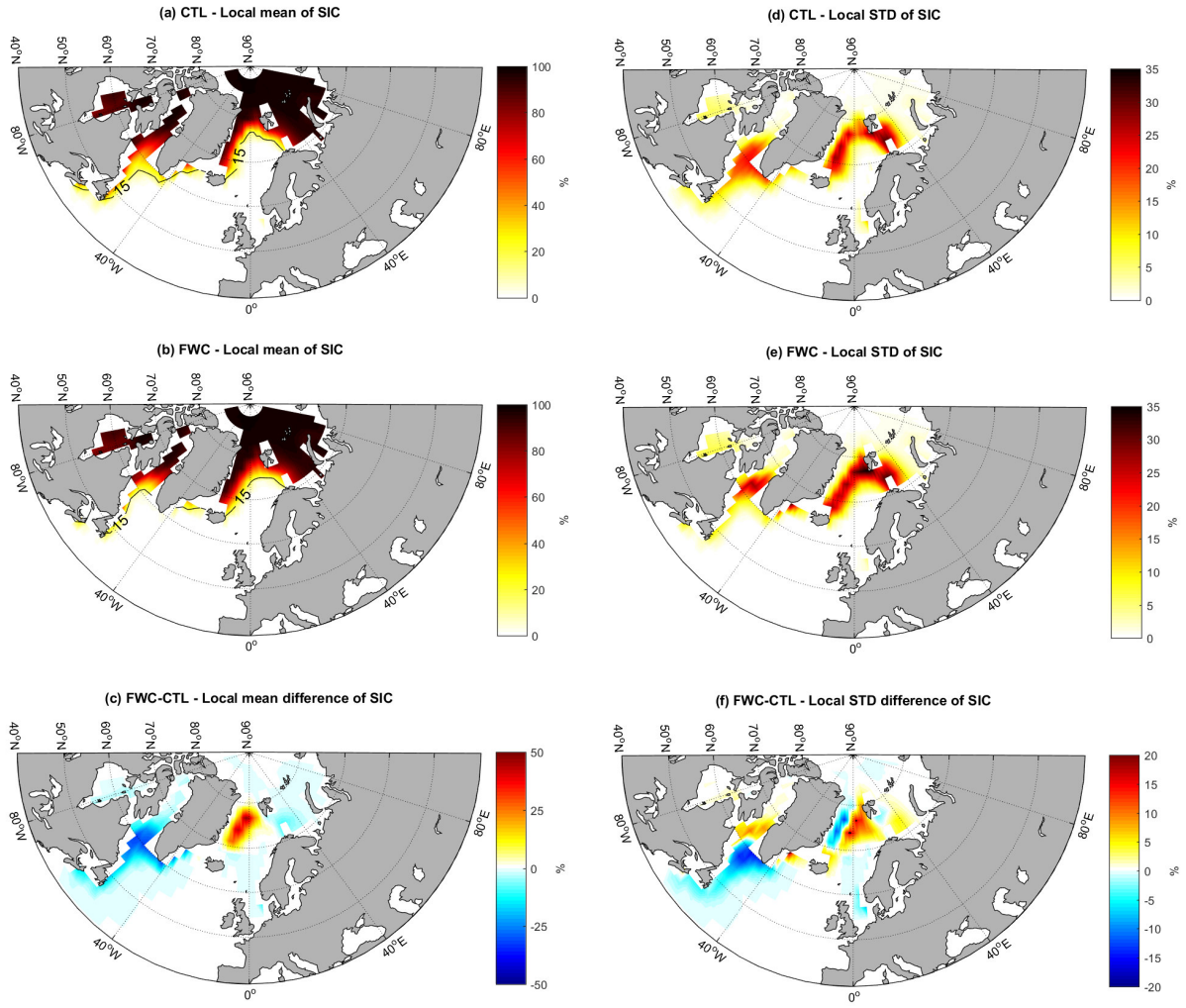

Fig. 1: Local mean and local STD of sea ice concentration for CTL are shown (a, b). FWC's mean and STD of sea ice concentration are depicted (d, e). The differences FWC-CTL of both quantities are shown in (c, f). The 15 % edge for sea ice is marked with a black line in (a) and (b).

in the GS fits the finding that the GS is gaining sea ice and extending its sea ice edge to the east. Also, a declining trend in SIC in the BS matches a decrease in SIC relative to CTL. Nevertheless, in relation to the overall SIA in the Atlantic sector of the Arctic these trends are small for the investigated time period. For 700 years the exerted trend in CTL is about $-1.2 \cdot 10^5\ km^2$ which refers to a decline of less than 2 % compared to the mean of $6.5 \cdot 10^6\ km^2$. The overall exerted trend of $-5.8 \cdot 10^4\ km^2$ per 700 years in FWC is substantially lower which confirms the improvement in model stability in comparison to CTL.

A correction of North Atlantic SSS seems to change the mean state and the local trend, especially in the LS, GS and BS. To further investigate the impacts on SIC variability and the influence on the climate system, EOF analyses are performed next.

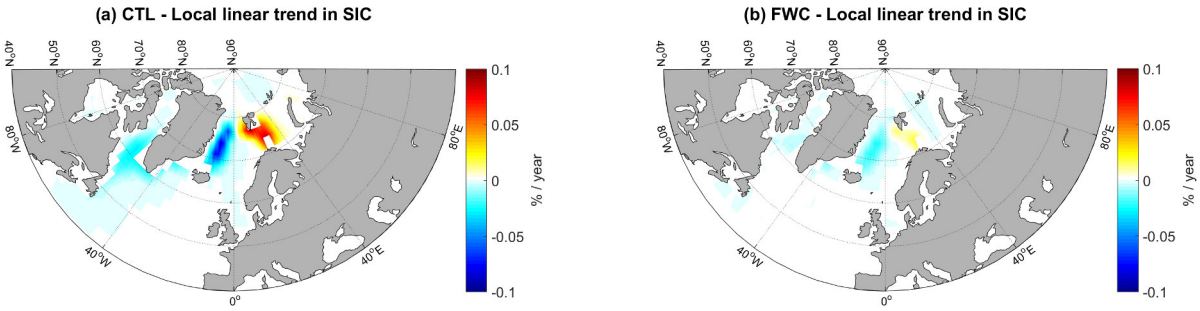

Fig. 2: The local linear trends in SIC for CTL (a) and FWC (b) are shown.

3.2 EOF analyses

Internal variability examinations using EOF and PC[9] require detrended time series data. For this purpose the local trend has been removed. EOF1 for CTL and FWC (Fig. 3a, b) show differences in the phase and the amplitude of the variances. Relative to CTL there's an enhancement in the representation of the joint phase for the GS and the BS. On the other hand, there is still no match with observations as the phase of the LS is represented incorrectly. CTL features a dipole pattern between in-phase centres of actions in the LS and GS and an out-of-phase centre of action in the BS. FWC shows a monopole in all of these three regions. Further, the amplitudes in FWC are reduced in the LS and GS. Both EOF patterns don't coincide with observations of *Deser et al.* (2000), *Singarayer et al.* (2003) and *Frankignoul et al.* (2014). They suggested a seesaw with in-phase centres of action in the GS and the BS and an out-of-phase centre of action in the LS as the leading mode of SIC variability. The mischief to correctly resolve the LS in FWC could be due to the massive sea ice loss there. Further, an improvement in explained variance compared to CTL is stated. The explained variance of roughly 60 % in CTL is a lot higher than that of FWC with about 40 %. *Deser et al.* (2000) found an explained variance of roughly 35 % for their leading mode of SIC variability which compares better to FWC than to CTL.

The corresponding PCs (Fig. 4a, b) show a different behaviour likewise. An enhancement in FWC relative to CTL is found since CTL features a regime shift at around year 1500 that is not found in FWC. An examination of two sub-periods of CTL is suggested due to the regime shift. CTL's PC displays a significant leap from negative to positive values around year 1500. This is indicative of an event taking place around that time and having a huge impact on the SIC variability, namely causing a persistent regime shift. Also, there still seems to be a trend in the time series of the PC that causes the PC to constantly rise. The PC of FWC doesn't feature either a leap or a trend and it appears to be more consistent and to have higher amplitudes. Since the PC of CTL

[9]In the following all of the PCs are normalised with their STD

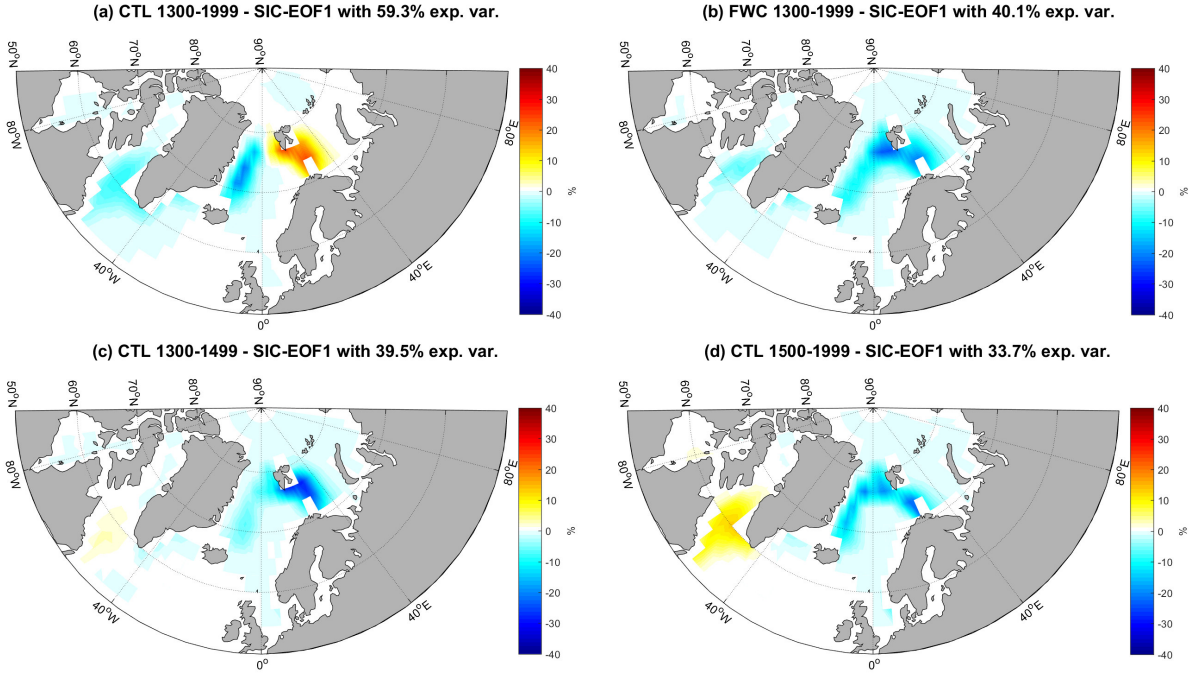

Fig. 3: Leading EOF patterns for CTL and FWC (1300-1999) are shown (a, b). Leading EOF patterns for CTL's sub-periods for the years 1300-1499 and 1500-1999 are depicted (c, d).

appears to be quite steady before and after the leap, this is strengthening the idea of a regime shift. As the noted regime shift adversely affects CTL's EOF analyses, CTL is divided into two sub-periods: A first time period before the regime shift from year $1300-1499$ is introduced, assessed and then compared to a second time period after the regime shift from year $1500-1999$.

A clear improvement by separating the full period into two sub-periods can be stated. EOF analyses for both sub-periods show an improvement in the EOF pattern. The first sub-period features a degradation concerning the variances' amplitudes, whereas the second period features an improvement. Both periods (Fig. 3c, d) outline a joint response in the GS and BS accompanied by a signal of opposite sign in the LS which fits the observed seesaw by *Deser et al.* (2000), *Singarayer et al.* (2003) and *Frankignoul et al.* (2014). The amplitudes of the first period's variances have decreased in all places compared to the full period. The strong signal in the BS and the coinciding weaker signals in the LS and GS can be explained by a poor choice of the first sub-period's time interval since the suggested regime shift starts just before year 1500 so that this period is also influenced by the regime shift. This can be linked to the local trend of the first sub-period (see App. Fig. 13c). The trends in SIC in the LS and GS have almost completely disappeared but the significant trend in the BS is still persisting. The post-regime shift period's response depicts a strong positive signal in the LS in association with an almost equally strong

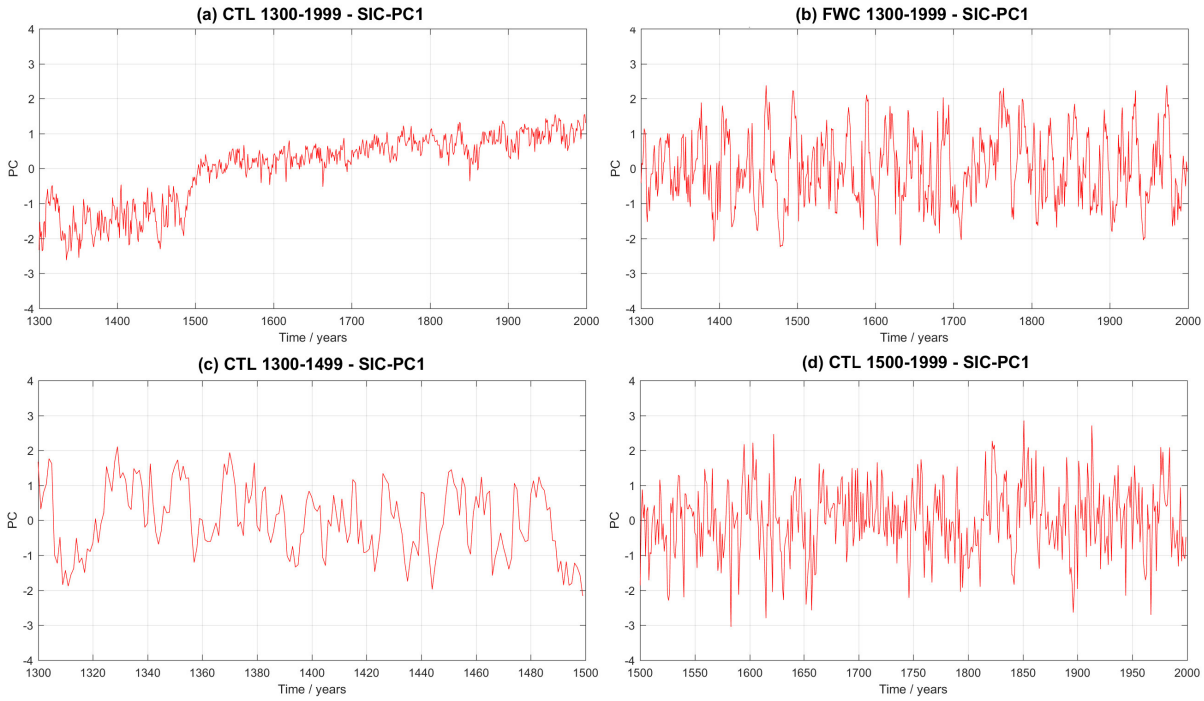

Fig. 4: Corresponding leading PCs for CTL and FWC (1300-1999) are shown (a, b). Leading PCs for CTL's sub-periods for the years 1300-1499 and 1500-1999 are depicted (c, d)

negative signal in the GS and BS. The full period's amplitudes of the variances have slightly increased. This compares well to the local trends (see App. Fig. 13f). The trend in the BS's SIC is very low such that this period doesn't seem to be influenced by the choice of the time interval. Both of the corresponding PCs (Fig. 4c, d) support an improvement relative to the full period since they are more consistent over time (no leap or trend). Further, the explained variances of approximately 40 % (pre-regime shift period) and 35 % (post-regime shift period) compare well to the mentioned 34 % by *Deser et al.* (2000).

To reveal the leading atmospheric mode responsible for the SIC variability, correlations[10] between SIC-PC1 and the local SLP and SAT[11] are carried out (later also: SIC-PC2 and SIC-PC3). These findings are compared to the leading wintertime SLP variability modes (see App. Fig. 14) and their well-known impacts on SAT. The leading mode is the NAO and explains almost 60 % of winter SLP variability for both, CTL and FWC. The second mode corresponds to the Barents Oscillation (BO) introduced by *Skeie* (2000) and *Chen et al.* (2013). The BO is characterised by positive pressure

[10] All of the EOFs, PCs and correlations are summarised in one respective figure for better comparison in the App. (Fig. 15, Fig. 16, Fig. 17 and Fig. 18)

[11] In order to maintain data consistency regarding SIC, the local trend of SLP and SAT has also been removed

data	EOF no.	exp. var.	SIC pattern	suggested atm. mode
observations	1	35%	dipole LS - GS/BS	NAO
CTL 1300-1499		40%	dipole LS - GS/BS	NAO
CTL 1500-1999		34%	dipole LS - GS/BS	NAO
CTL 1300-1999		60%	dipole LS/GS - BS	(RBO)
FWC		40%	monopole LS/GS/BS	(NAO)
observations	2	12%	dipole LS/BS - GS	AO
CTL 1300-1499		16%	dipole LS/BS - GS	RBO
CTL 1500-1999		25%	monopole LS/GS/BS	AO
CTL 1300-1999		13%	dipole LS - GS/BS	NAO
FWC		20%	dipole GS/BS	(RBO)
observations	3	n.a.	n.a.	n.a.
CTL 1300-1499		14%	monopole LS/GS	AO
CTL 1500-1999		9%	dipole LS/BS - GS	RBO
CTL 1300-1999		9%	monopole LS/BS	AO
FWC		9%	monopole LS	AO

Tab. 1: Overview of obtained results regarding the EOFs and atmoshperic drivers. Explained variance, SIC pattern and the suggested atmospheric mode are shown for the different datasets. EOF1 observations and findings originate from *Fang et al.* (1994), *Deser et al.* (2000), *Singarayer et al.* (2003) and *Frankignoul et al.* (2014), EOF2 findings from *Singarayer et al.* (2003) and *Aue* (2016). Findings that can not finally be conceded are in brackets.

anomalies over the Barents Sea and resulting positive SAT anomalies over the GS and BS. The third atmospheric mode seems to be less regarded in literature, possibly due to its minor effects on the large-scale circulation. It resembles the BO (sign reversed) with the negative center of action more westerly between Iceland and Scandinavia and an extra positive spot further north. From here on, it will be called RBO (reversed BO).

All of the the results that are conceded from the correlations are summarised together with the findings of the EOF analyses in Tab. 1. From observations *Fang et al.* (1994) and *Deser et al.* (2000) found the NAO as atmospheric driver for the leading mode of SIC variability. Especially versatile wind forcing, oceanic heat transport and surface heat exchange were made responsible for being the causes (*Fang et al.*, 1994). Correlations for CTL's full period can't prove this result as no final evidence for any atmospheric mode can be inferred. This isn't surprising as the SIC variability pattern doesn't match the observed pattern either. The two sub-periods' correlations favour the NAO as the driving force and support observations. Further, this shows that CTL's representation of Arctic SIC variability is perturbed by the noted regime shift. Compared to the sub-periods, FWC can't confirm the NAO or any of the aforementioned atmospheric modes as driver for its leading EOF pattern which concludes a degradation of SIC variability that is evoked by the performed SSS correction.

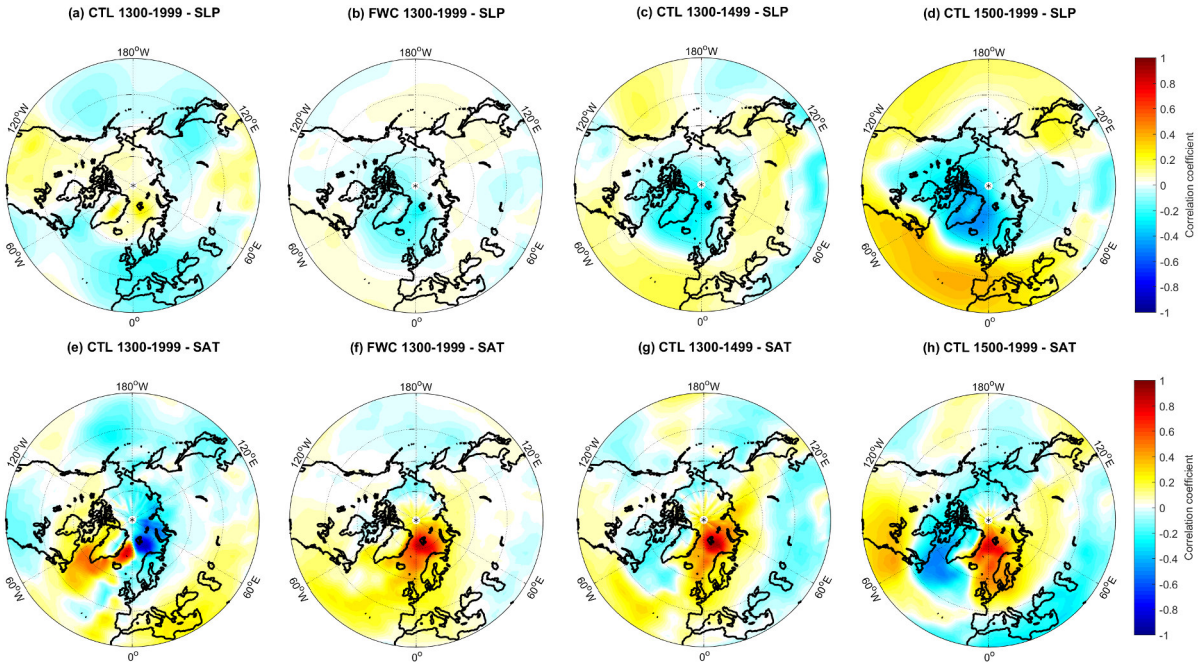

Fig. 5: Correlations of SIC-PC1 with local SLP for CTL's full period (a), FWC (b) and CTL's two sub-periods (c, d) are shown. Correlations with the local SAT for the respective time periods are depicted (e-h)

The correlations yield different outcomes. The full period of CTL combines a high pressure anomaly over the central Arctic with low temperatures over the BS and high temperatures over the LS and GS (Fig. 5a, e). An interpretation of the prevailing atmospheric mode appears difficult as there is no clear link to either the NAO, AO or BO. It slightly resembles the RBO pattern but the centres of action don't coincide well because the negative SLP anomaly is located too far to the south and is too extensive. A conspicuous positive correlation with the SAT at the east coast of Greenland is marked.

In spatial pattern the sub-periods' correlations are similar to each other, but the second period's amplitudes are higher. SLP correlations (Fig. 5c, d) display a dipole between the Arctic and the mid-latitudes. The centre over the Arctic is more extensive than the one of the full period. An almost closed zonal ring separates negative values from positive ones. The SAT patterns (Fig. 5g, h) show positive correlations over parts of Asia, Northern Europe and east of Greenland in the GS and BS, whereas Greenland itself, the LS and northeast Canada feature negative correlations. These findings favour the NAO as the leading atmospheric mode driving the SIC variabilities. Stronger-than-normal north-to-south SLP gradients allow increased SAT in the GS and BS and yield high SAT correlations with the respective negative signal of EOF1 leading to a decreasing in the SIC. Analogous cold temperatures in the LS caused by an enhanced export of heat result in negative SAT correlations with the positive signal in EOF1 and an increase in SIC.

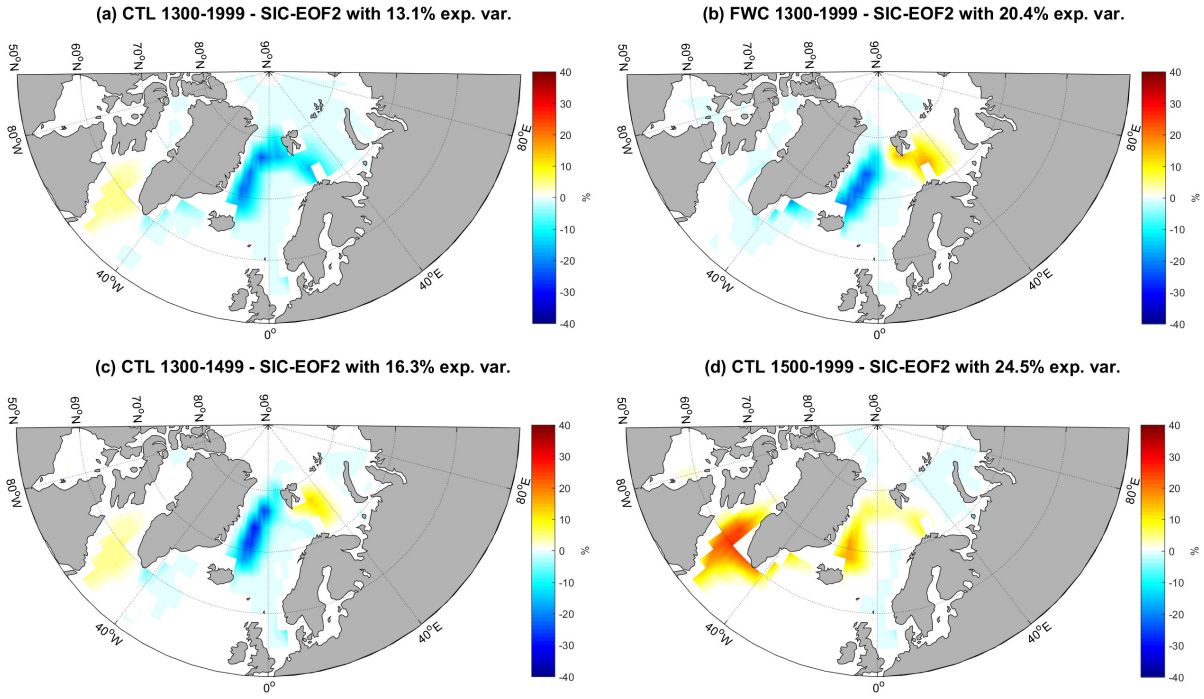

Fig. 6: Second EOF patterns for CTL and FWC (1300-1999) are shown (a, b). Second EOF patterns for CTL's sub-periods for the years 1300-1499 and 1500-1999 are depicted (c, d).

Compared to CTL (all periods), FWC doesn't feature notably high correlations with SLP. There might be a slight indication for a NAO-like mode in the SLP and in the SAT correlations (Fig. 5b, f). A negative pressure centre over Greenland and positive anomalies around the Atlantic mid-latitudes with combined positive SAT correlations over Europe and the GS/BS could be indicative but no negative signal in the LS region is to be noted. Moreover, it should be minded that the SLP signals are too low to concede a final answer here.

As mentioned in Sect. 2.3.4, analyses of higher order EOFs have to be interpreted carefully. Due to their restrictions to orthogonality the relevance for physical processes decreases with higher order. The second EOFs are displayed in Fig. 6. For an overview of the respective third EOF patterns, PCs and correlations see the Appendix (Fig. 15, Fig. 16, Fig. 17 and Fig. 18). From the results it can be concluded that there are multiple processes involved which confuse the SIC variability in terms of intensity and phase and also the associated mode's order for all of CTL's periods and also for FWC. Further, FWC mostly fails to resolve the LS correctly and to present perceptible atmospheric drivers such that no improvement relative to CTL can be stated. Evidences for the AO and hints for the RBO as atmospheric drivers of SIC variability can be found.

CTL's full period EOF2 features the SIC pattern induced by the NAO (Fig. 6a). Also, the corresponding correlations with SLP and SAT (see App. Fig. 17h and Fig. 18h) show

clear evidences for the NAO being the driver of this SIC variability mode. The second EOF of FWC shows a different pattern. It resembles EOF1 of CTL's full period but without the signal in the LS. Moreover, there's a peak in the corresponding PC around year 1700 (see App. Fig. 16k) that disappears after 50 years such that a permanent regime shift can be excluded here. The similarity to CTL's EOF1 is supported by the corresponding correlations with SLP and SAT (see App. Fig. 17k and Fig. 18k) which possibly give a hint to the RBO. A stronger indication of the RBO as a driver is shown by CTL's first period. The associated SLP correlation (see App. Fig. 17b) displays anomalous low pressure between Iceland and Scandinavia which compares well to the described SLP variability of the RBO. The only period to find the AO as the driver of the second mode of the SIC variability, is the second period of CTL. The corresponding correlation with SLP (Fig. 17e) yields an AO-like pattern with low pressure over the central Arctic and Greenland and high pressure over the Azores and the Aleutian Islands. The SAT correlation (Fig. 18e) coincides well with the AO temperature signatures. There are positive values to be found over large parts of the Eurasian continent and negative values over northeast Canada. EOF3 is dominated by the AO and the AO-induced EOF pattern except for the second period of CTL that features a weak RBO signal. As to be seen in Tab. 1 some of the EOF patterns appear to be mixed up in their order, probably due to the regime shift. Since the second period of CTL seems to be unaffected by the regime shift and it confirms the AO as second leading atmospheric driver of SIC variability, it is the most stable period.

3.3 Sea surface salinity as driver of sea ice concentration variability

After *T. Park et al.* (2016) the AMOC index is represented more realistically in FWC compared to CTL. Figure 10 in *T. Park et al.* (2016) shows that there's an enhancement in the amplitude and variability of the AMOC. In FWC there's a rapid increase to be seen around year 1700. It is followed by a significant decrease around 1750. The AMOC's variability in CTL is less distinct than in FWC but also features one substantial peak at year 1450 where it rapidly drops and increases again. Both of the stated peaks temporally coincide with the mentioned noticeable peaks in PC1 of CTL (Fig. 4a) and PC2 of FWC (Fig. 16k). In order to assess the question if the AMOC could be the reason for these peaks, for the suggested regime shift in CTL and possibly for the unlike EOFs, the sea ice area in the LS, GS an BS is analysed. By this method the direct impact of the AMOC on SIA can be estimated as an increased AMOC yields enhanced SST in the Northern Hemisphere mid- and high-latitudes (*Knight et al.*, 2005) and thus effects SIC (and also SIA) (*van der Swaluw et al.*, 2007; *Semenov, Latif, Dommenget et al.*, 2010).

As to be seen in Fig. 7a there's a change in CTL's SIA around year 1500 in all of the three defined areas. The LS's SIA drops by almost $0.5 \cdot 10^4$ km^2 within 50 years. The

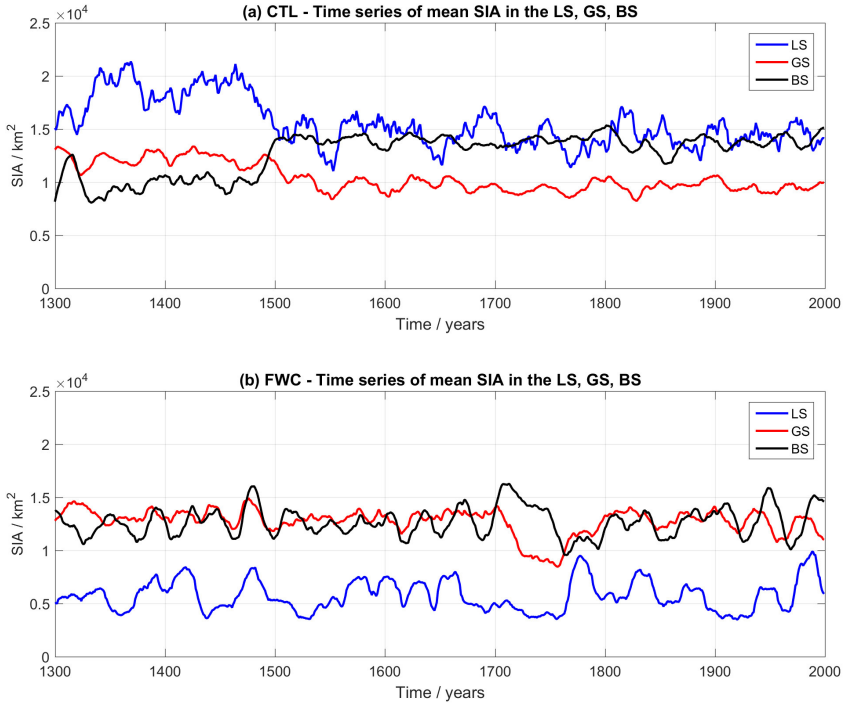

Fig. 7: Regional mean SIA for CTL (a) and FWC (b) with the colour coding in the panels. The data is processed with a 10-year running mean.

GS's SIA shows less a distinct response but a slight decrease is visible. A rapid increase in SIA from $1.0 \cdot 10^4$ km^2 up to $1.5 \cdot 10^4$ km^2 in the BS is noticeable. Most significant is the fact that the changes in SIA remain in force after the AMOC regularised. This pattern compares very well to CTL's pattern of EOF1 (Fig. 3a) such that this behaviour seems to be responsible for the major SIC variability in CTL (full period). This phenomenon - the regime-like shift in SIA with a seesaw between the GS and the BS - was described by *Semenov, W. Park et al.* (2009) and *Smedsrud et al.* (2013) as Barents Sea Inflow (BSI) shutdown. The BSI shutdown is recognised to cause rapid climate transitions in confined areas - namely the northern high-latitudes - without significantly effecting the global climate. It is based on a positive feedback between warm waters carried into the BS by the North Cape Current and surface near westerly winds. If less heat is brought into the BS by the North Cape Current, the formation of sea ice is favoured. Further, the atmosphere is cooled by the ocean and an anti-cyclonic circulation anomaly is forced which yields an increase in SLP in the BS. This phenomenon refers to the third mode of SLP variability (Fig. 14c, i), the RBO. The increase in SLP is accompanied by less strong surface westerly winds. These winds increase the perturbation of water inflow into the BS (and thus the heat inflow). As a consequence, the Atlantic surface waters can't enter the BS and re-circulate along the east coast of Greenland. While SAT drops in the BS, the re-arranged ocean circulations warm the GS and yield positive temperature anomalies

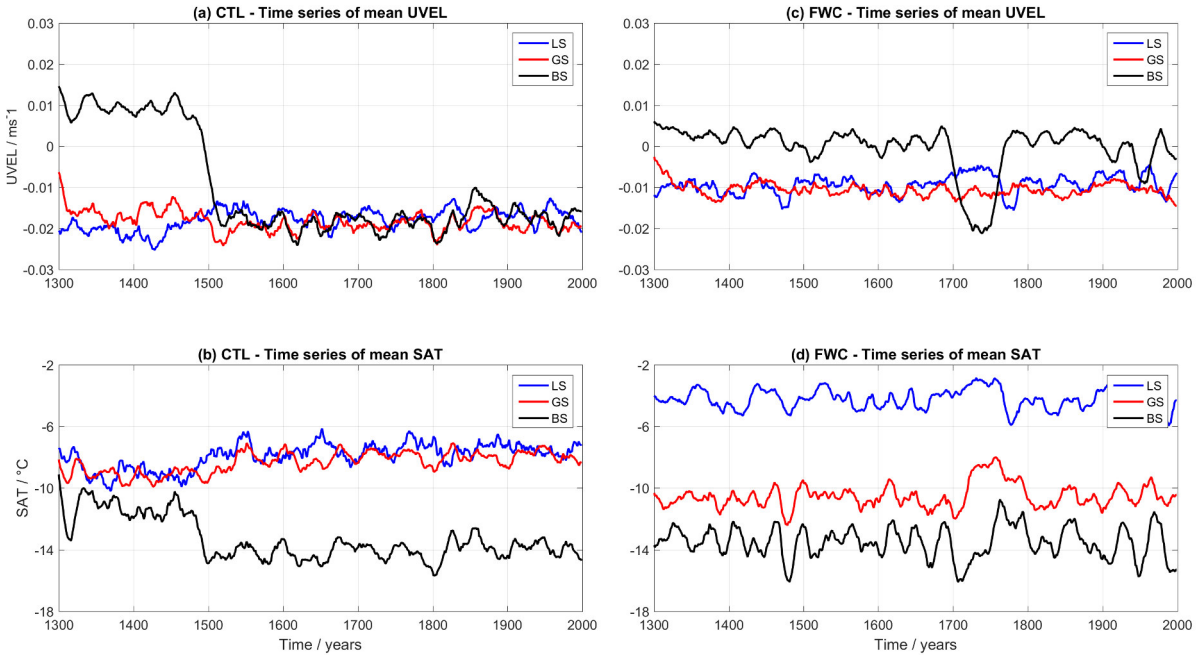

Fig. 8: Regional mean UVEL for CTL (a) and FWC (c) with the colour coding in the panels. Mean SAT for CTL (b) and FWC (d). The data is processed with a 10-year running mean.

(*Semenov, W. Park et al.*, 2009). To trigger this climate tipping point anomalous cool conditions have to be provided. Primarily the atmospheric circulation in the in form of NAO (*Dickson et al.*, 2000; *Kwok*, 2000) and SLP gradient between North Cape and Svalbard (*Bengtsson et al.*, 2004) are regulating this trigger but it is also influenced by the multi-decadal variability of the AMOC (*Bengtsson et al.*, 2004; *Semenov, Latif, Jungclaus et al.*, 2008). If excessive heat is carried into the BS the prevailing climate may tip back to its previous conditions.

Since the AMOC minimum of CTL temporally coincides with a change in sign of the mean zonal component of the surface ocean current (UVEL) in the LS (Fig. 8a), a shutdown of the BSI, triggered by the AMOC is suggested. The associated persistent SAT decrease in the BS and increase in the GS (Fig. 8b) fit the anomalies found by *Semenov, W. Park et al.* (2009). The rise in SAT in the LS seems to be connected to the BSI shutdown as the characteristics match in time but it is not further investigated here. Correlations performed with mean UVEL in the LS (Fig. 9a-c) show significant similarity (sign reversed) to the the first EOF of CTL (Fig. 3a) and to the correlations with SLP and SAT (see App. Fig. 17g and Fig. 18g): A normal state would inhibit positive zonal velocities and connected to that are heat transport into the BS, increased SAT and sinking SIC. In reverse, a state of BSI shutdown with negative velocities would inhibit correlations with the sign reversed and thus rising SIC. It remains unresolved why the SAT correlation is in combination with a BO-like SLP pattern instead of RBO.

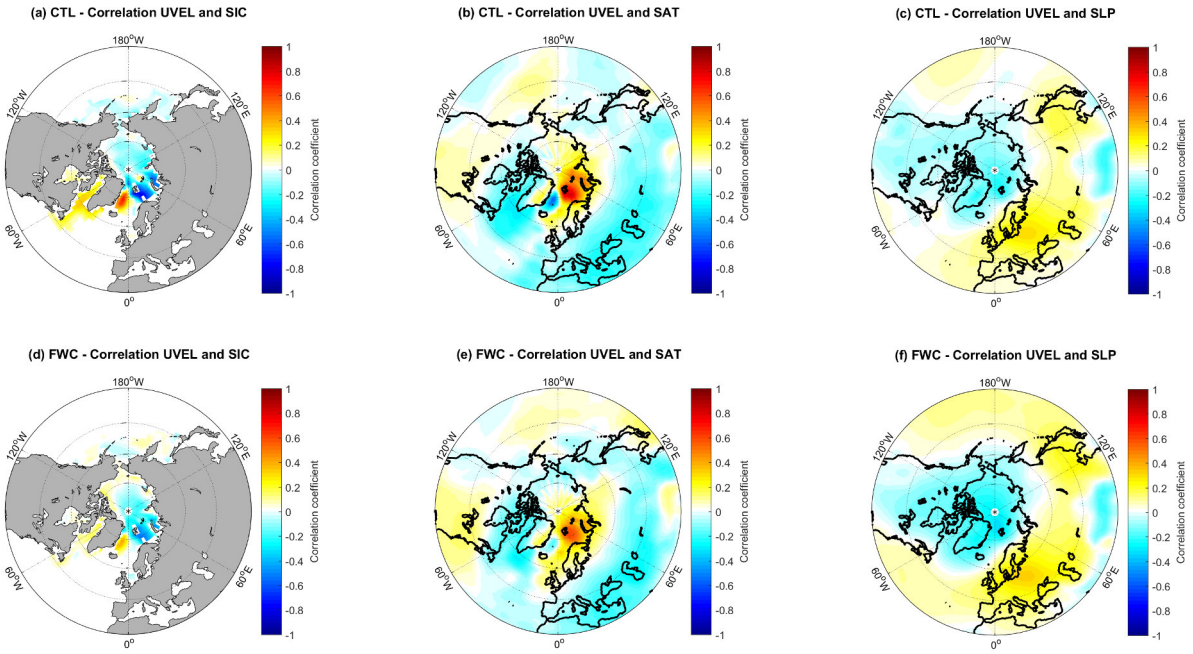

Fig. 9: Correlations of CTL's mean UVEL with SIC, SAT and SLP (a-c). Correlations of FWC's mean UVEL with SIC, SAT and SLP (d-f).

At this point, it can be concluded that the first mode of the SIC variability in CTL's full period is governed by a BSI shutdown as shown by the SIC and SAT patterns but the atmospheric driver can not finally be found. Also, the two introduced sub-periods of CTL seem to be influenced by the BSI shutdown which is especially shown by the SAT correlations (Fig. 18b, f). The pre-regime shift period is probably affected due to the choice of the time interval that coincides with the AMOC event. The post-regime shift period might be affected due to the persisting conditions like a decreased SAT in the BS or a reversed zonal velocity component.

In comparison to CTL, FWC does not feature a negative peak in the AMOC index. Fig. 7b consequently shows that there is no regime shift in SIA either. Surprisingly, Fig. 8c states a loss in mean UVEL in the BS for approximately 50 years from year 1700 on. This indicates a BSI shutdown for FWC which might be due to atmospheric and not to oceanic influence. The subsequent peak in the AMOC index - whether forced randomly at the same time or caused by an unknown feedback - appears to be responsible for the tip-back by delivering enough heat into the BS region. The SIA signal (Fig. 7b) and the associated SAT response are relatively weak compared to CTL. If closely looked, a slight decrease in the BS's SAT and an increase in SIA can be noticed as well as a decrease in SIA in the GS caused by enhanced SAT just around year 1700. It is supposed that the lack of SIA response and the less distinct SIC correlation in the LS (Fig. 9d) relative to CTL are due to the shortness of the BSI shutdown. These findings coincide with EOF2

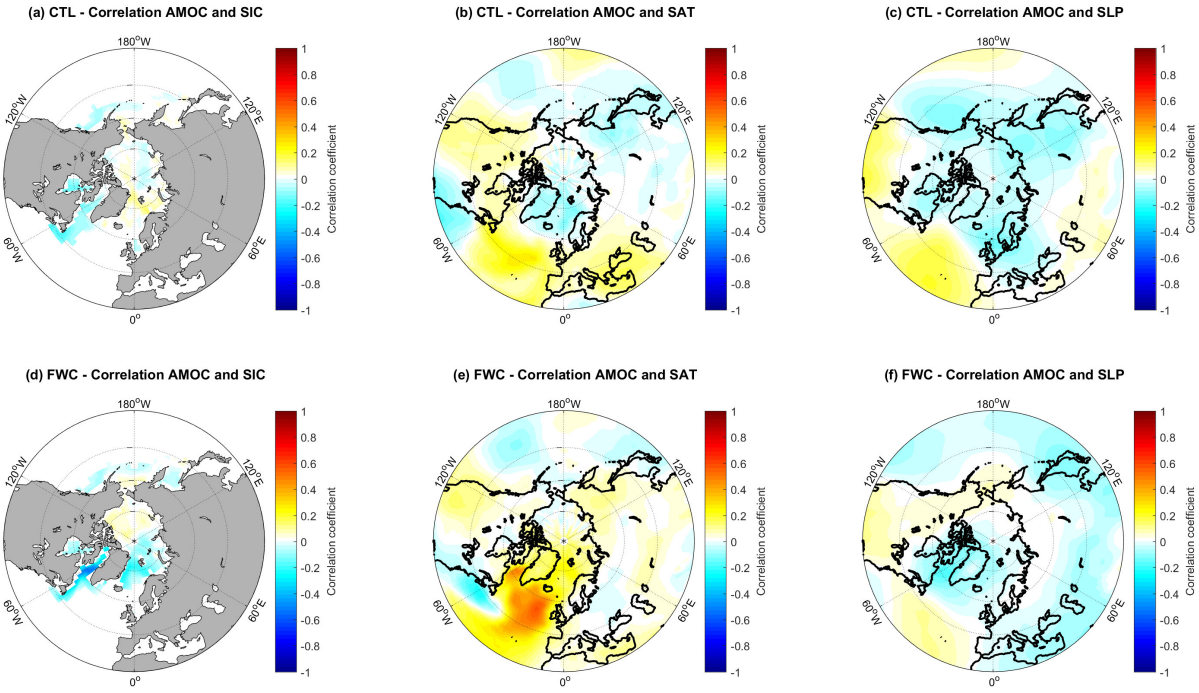

Fig. 10: Correlations of CTL's AMOC index with SIC, SAT and SLP (a-c). Correlations of FWC's AMOC index with SIC, SAT and SLP (d-f).

of FWC. Thus it can be stated that a BSI shutdown - with a less long presence than in CTL - governs the second EOF mode of SIC variability in FWC.

Left for explanation is the leading mode of FWC. The aforementioned weak NAO-like response in EOF1 with a missing negative anomaly in the LS is now further investigated by analysing the impact of the AMOC on the local SAT and the atmospheric circulation. As to be seen, a major gap in the impact of the AMOC on the SAT between CTL and FWC is exhibited (Fig. 10b, e). FWC's signal in the mid-latitude Atlantic and especially in the LS is significantly higher and extends to the pole. In CTL there's a negative response to be seen starting south of Greenland extending to the pole. The respective patterns in SIC relate to this finding (Fig. 10a, d). A weak dipole in CTL and a stronger monopole in FWC can be seen such that a change in the amplitude and phase of the SIC signal is achieved in FWC. The monopole with centres of action in the LS, GS and BS and its maximum in the LS fits the results of *T. Park et al.* (2016) (sea ice loss of up to 40 % in the LS). This outcome seems to be inevitably connected to the strengthened AMOC evoked by the SSS correction. *T. Park et al.* (2016) suggested that a northward extension of the subtropical gyre and a more northern position of the North Atlantic Current could be the cause for SAT warming in FWC. Fig. 10e shows that a considerable portion of this warming is due to the increased AMOC. Further, an impact on the north-to-south SLP gradient is noticeable (Fig. 10c, f). The correlation in FWC yields less strong values in all places such that a negative influence of the AMOC on the

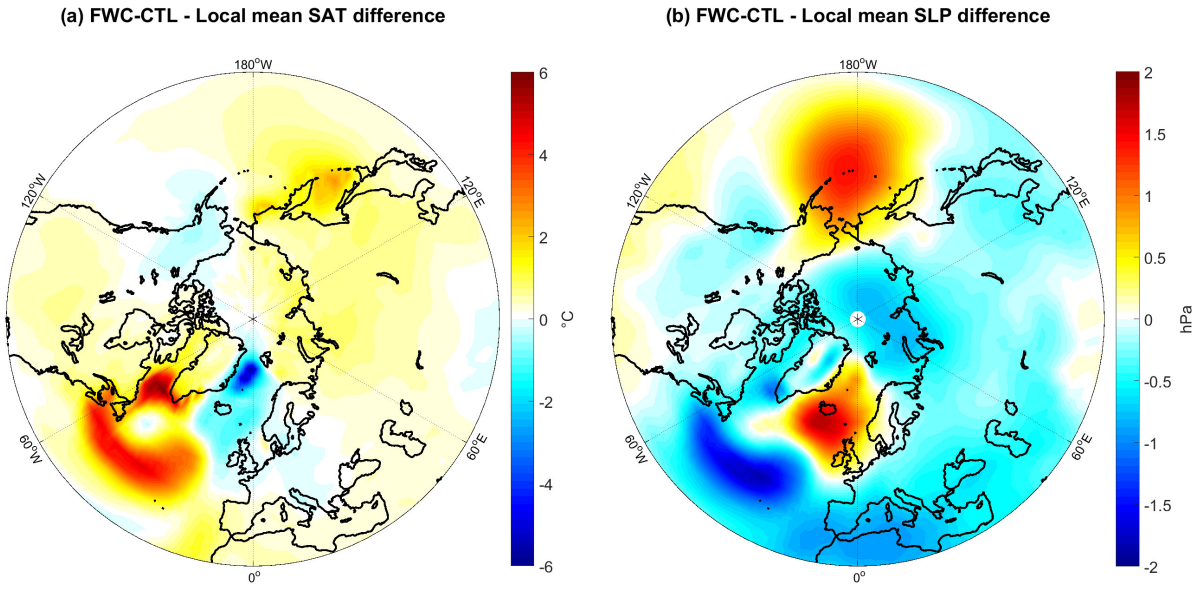

Fig. 11: Difference FWC-CTL for the mean SAT (a) and SLP (b).

prevailing atmospheric circulation is suggested. Fig. 11 depicts the difference in mean SAT and SLP between FWC and CTL and confirms the aforementioned warming of the Atlantic and LS as well as a reduced SLP gradient. In contrast to the LS, the GS is cooling down relative to CTL which is surprising because it is found that an increased AMOC leads to a warming in this area (Fig. 10e). As a consequence, another process must be responsible for the GS's cooling, for example the shorter-lasting BSI shutdown event in FWC with a shorter period of warming for the GS relative to CTL. Connected to the SAT change there's a change in SLP. Increased temperatures over the Atlantic lead to a decrease in the corresponding SLP. The contrary manner is observed over the GS and between Iceland and Scandinavia. This reduction in the SLP gradient coincides with the result of *T. Park et al.* (2016) who suggested that this could reduce a positive bias in comparison to observations. After *Keeley et al.* (2012) this reduction of the bias also leads to a weakened NAO but which - although confirmed in a fraction of amplitude (Fig. 12c) - is negligible in terms of SAT impacts. Also, the SLP variability modes support this result as there are no large differences in spatial pattern and explained variance (see App. Fig. 14). It results that there are no significant changes in the mean circulation due to the SSS correction which in turn means that the increased AMOC is gaining influence on SAT and SIC variability relative to CTL. It is suggested that the leading mode of SIC variability of FWC is governed by a combination of NAO and AMOC. The distinct positive SAT anomaly over the GS and BS (Fig. 5f) is NAO-induced while the negative signal in the LS is masked by an enhanced influence of the AMOC in this region. The SLP response compulsorily is reduced as an outcome of the combination of these two drivers.

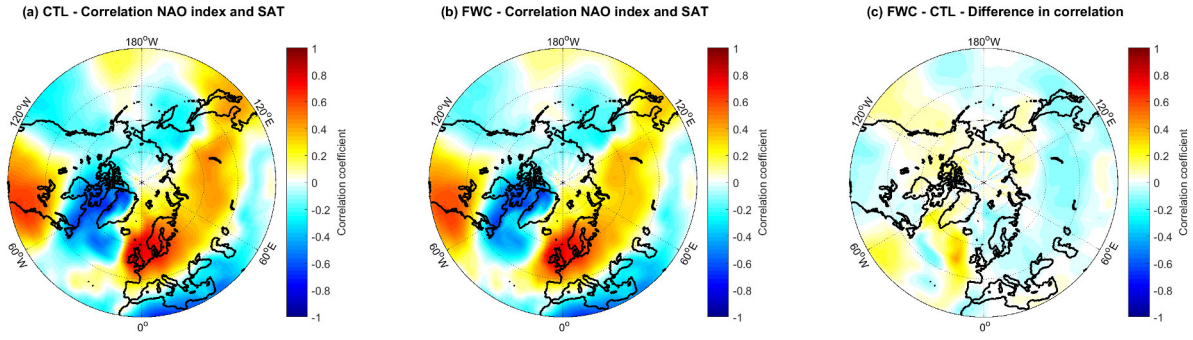

Fig. 12: Correlations of the NAO index with the SAT for CTL (a), for FWC (b). The difference FWC-CTL is depicted in (c).

Finally, it can be concluded that the AMOC is responsible for the noticed peaks in the PCs, the regime shift and also for the lack of CTL and FWC to match observed SIC variability modes. Evoked by a larger bias in SSS, CTL is more prone to a climate tipping point than FWC. In contrast to CTL, FWC is able to regulate this tipping on its own. The reduction in the SSS and SST biases, enhanced the AMOC characteristics but a connected rise in SAT degrades SIC variability, especially in the LS.

4 Discussion

T. Park et al. (2016) performed a SSS correction in the North Atlantic sector of a control run of KCM. They found this correction to be alleviating a well-known SSS bias in high latitudes and subsequently an enhancement of the AMOC. This led to a reduction of SST and SLP biases but also to a degradation of Arctic sea ice simulation. In this study the impact on SIC variability and relevant atmospheric and oceanic parameters relative to the control run were investigated.

Mean state analyses confirm shrinking sea ice concentration in the LS relative to the control run which is an improvement, as CTL is characterised by excessive sea ice in this region. On the opposite, the GS gains sea ice compared to CTL but a net loss of SIC in the Atlantic sector of the Arctic is stated such that the positive SIC bias could be reduced. Further improvement results from local linear trend analyses which show that the regional and the overall trends are reduced for the benefit of model stability. EOF analyses and corresponding correlations (see App. Fig. 15, Fig. 16, Fig. 17 and Fig. 18) show an influence of the SSS correction on SIC variability. The spatial pattern in the GS and in the BS is almost the same in both integrations. Due to the massive sea ice loss in the LS, FWC mostly fails to resolve a signal in the LS. As a consequence of the sea ice loss, the associated atmospheric drivers (NAO, RBO, AO) and their impacts on the SAT are similar to CTL but weaker. The order of CTL's and FWC's modes mix up in the wake of a regime shift (BSI shutdown) taking place in both integrations. This is confirmed by comparing the two integrations to a sub-period of CTL which is the best fit for observations.

Observational data favour the NAO as the leading mode of SIC variability linked to a seesaw between the LS and the GS/BS (*Deser et al.*, 2000; *Singarayer et al.*, 2003; *Frankignoul et al.*, 2014). For the second mode, *Aue* (2016) suggested the AO as driver. The EOF pattern features a seesaw between the LS/BS and the GS (*Singarayer et al.*, 2003; *Aue*, 2016). Additional second (and also third) EOF analyses with sufficient matching parameters were not be found in literature. Some analyses examined summer time EOF while others remained uncommented or were said to be artefacts (*Partington et al.*, 2003).

CTL's (full period) EOF1 doesn't feature the described NAO-induced pattern. It features a seesaw between the GS and BS as the leading mode of SIC variability. This is not surprising, as CTL is affected by a regime shift. The corresponding PC depicts a markedly leap that is indicative of the regime shift around year 1500. The SLP correlation shows an atmospheric pattern that can't finally be referred to any of the introduced patterns but SAT correlations favour the RBO. The second and third EOF are driven by NAO and AO and yield the described EOF patterns. The sub-periods of CTL show similar signals for all of their three calculated EOFs. The first mode is governed by a

dipole between the LS and the GS/BS. The pre-regime shift period shows less distinct amplitudes relative to the post-regime shift period. This might be very well due to the bad choice of the time interval. Correlations with SLP and SAT yield NAO patterns. The second and third EOFs look alike but with the order changed. This swap of the EOFs might also be due to the influence of the regime shift on the first period. EOF2 for the first and EOF3 for the second period show a seesaw of nearly same amplitude between the LS/BS and the GS. The atmospheric correlations show indications of the RBO with centres of action over Iceland and Scandinavia as well as Southern Europe. The related SAT correlations show a cooling over the BS and a conspicuous warming over the GS. EOF3 for the first and EOF2 for the second period depict a monopole with the maximum response in the LS. According to correlations this pattern is induced by the AO.

The leading mode of SIC variability for FWC shows an improvement in the GS and BS (joint phase) but a degradation in the LS compared to CTL as there is no strong signal in the LS. Correlations show a weak NAO-like signal but without the typical negative response in the LS. Analyses show that an increased AMOC yields an increase in SAT in the LS region so that a combination of NAO and AMOC is suggested for the leading mode of SIC variability in FWC. The second EOF features the signatures of the BSI shutdown. Relative to CTL it is an improvement that - despite a regime shift - FWC features a NAO-like pattern as the first mode. At this point it should be noted that the shutdown event persisted for a longer time in CTL which might play a role for the SIC variability and the EOF's order. The third mode is AO-induced.

The post-regime shift period approves the observed atmospheric drivers. The NAO-induced EOF pattern can be confirmed, whereas the AO-induced pattern can't. One possibility for this mischief is the smaller but still existing SST bias: As to be seen in figure 24a in *Aue* (2016), considering solely the SAT pattern would exhibit the same SIC variability but in combination with the corresponding SST pattern (figure 24c) the driver for the observed signal can be found. CTL (full period) is hugely influenced by the shutdown event that accounts for the largest explained SIC variance. The NAO and AO follow with the second and third largest portions. FWC features a combination of NAO and AMOC and thus weak correlations with SLP. A shorter shutdown event and the AO account for the second and third largest portions.

Investigations of the AMOC yield a substantial higher influence on Atlantic SAT (Fig. 10b, e). Especially the LS, GS and BS are affected. The gain in heat in the Arctic regions relative to CTL results in a SIC response with a monopole in all of the three regions (Fig. 10d). This concludes a loss of total sea ice in FWC driven by the ocean. On the other hand, mean state analyses show a gain of SIC in the GS that in turn has to be caused by the atmosphere. The gain in SIC can be explained by a climate transition that occurs in CTL and FWC but persists and thus heats the GS for a shorter time in FWC.

In CTL this climate transition - found to be the Barents Sea Inflow shutdown (*Semenov, W. Park et al.*, 2009; *Smedsrud et al.*, 2013) - is triggered by an AMOC event. In FWC, no AMOC event coincides with the beginning of the BSI shutdown but a peak in the AMOC coincides with the ending of the BSI shutdown. A lower vulnerability of FWC to fall and remain in the shutdown phase is suggested. It is stated that the alleviated SSS bias is enhancing the AMOC's influence on Arctic climate.

From sea ice area and zonal velocity component data it results that the BSI shutdown begins around year 1500 in CTL and persists until the end of the investigated data in 1999. In FWC it is found to take place around year 1700 and lasts for only 50 years (Fig. 7 and Fig. 8). The BSI shutdown is accompanied by a decrease in UVEL and strongly impacts the near surface westerly winds in such manner that the perturbation of water inflow into the BS is further enhanced (*Semenov, W. Park et al.*, 2009). Water masses are forced to re-circulate along the east coast of Greenland and to carry the heat along. A regime shift in SIA is achieved: The resulting SAT cooling over the BS leads to an increase in SIC, and the rise in SAT in the GS leads to a decrease in SIC. The LS seems to react to these changes in the ocean and atmosphere as well, but no final conclusions regarding why and how were made by *Semenov, W. Park et al.* (2009) and neither did this study examine this topic. The less strong response of FWC concerning the LS's SIC signal during the BSI shutdown is probably due to the shortness of this event. It would be interesting to see if a longer BSI shutdown could exhibit an equally strong response as in CTL. A further implication of the BSI shutdown is a lower mean SAT over the GS in FWC due to a less long heating period. In combination with a stronger heating caused by the enhanced AMOC in the mid-latitude Atlantic, the resulting difference in mean SAT yields pressure anomalies of reversed sign over the respective areas (Fig. 11). This finding coincides with the aforementioned reduced SLP bias and concedes a weaker NAO (*Keeley et al.*, 2012) relative to CTL (Fig. 12). The amplitude of this difference is relatively small which is supported by EOF analyses for SLP: The NAO with almost the same spatial pattern and explained variance is the leading mode for CTL and FWC, followed by the BO and RBO (see App. Fig. 14).

In this work the extensive impacts of the SSS correction can be confirmed, for instance the reduction of a SLP bias or an enhanced influence of the AMOC on SAT. Going along with this is a lower vulnerability to fall into persistent climate transitions compared to CTL. With regards to SIC variability the SSS correction leads to a degradation relative to CTL. Due to excessive sea ice loss in the LS, FWC isn't able to resolve most of the observed SIC variability patterns there, so that the representation of Arctic sea ice remains an issue in KCM as stated by *T. Park et al.* (2016). Investigations of the processes causing the LS to react during BSI shutdown events, could hone the understanding of the driving forces of SIC variability. Furthermore, a combination of SAT and SST data could help to close the gap between the observed SIC and the simulated pattern induced

by the AO. In order to conduct future simulations for the Arctic, an improvement of the model in form of a flow field correction as carried out by *Drews et al.* (2015) is suggested. This could additionally reduce the subsurface bias in SST which could further enhance the model's quality in representing Arctic sea ice.

References

Aue, L. (2016): Mechanismen der Meereisvariabilität aus Beobachtungen. *Bachelor-Arbeit im B. Sc. Physik des Erdsystems: Meteorologie, Ozeanographie, Geophysik (an: Christian-Albrechts-Universität zu Kiel)*, 1–55.

Bader, J., Mesquita, M. D., Hodges, K. I., Keenlyside, N., Østerhus, S. & Miles, M. (2011): A review on Northern Hemisphere sea-ice, storminess and the North Atlantic Oscillation: observations and projected changes. *Atmospheric Research*, 101.**4**, 809–834.

Bengtsson, L., Semenov, V. A. & Johannessen, O. M. (2004): The early twentieth-century warming in the Arctic-A possible mechanism. *Journal of Climate*, 17.**20**, 4045–4057.

Chen, H. W., Zhang, Q., Körnich, H. & Chen, D. (2013): A robust mode of climate variability in the Arctic: The Barents Oscillation. *Geophysical Research Letters*, 40.**11**, 2856–2861.

Delworth, T. L. & Mann, M. E. (2000): Observed and simulated multidecadal variability in the Northern Hemisphere. *Climate Dynamics*, 16.**9**, 661–676.

Delworth, T. L., Rosati, A., Anderson, W., Adcroft, A. J., Balaji, V., Benson, R., Dixon, K., Griffies, S. M., Lee, H.-C., Pacanowski, R. C., Vecchi, G. A., Wittenberg, A. T., Zeng, F. & Zhang, R. (2012): Simulated Climate and Climate Change in the GFDL CM2.5 High-Resolution Coupled Climate Model. *Journal of Climate*, 25.**8**, 2755–2781.

Deser, C., Walsh, J. E. & Timlin, M. S. (2000): Arctic sea ice variability in the context of recent atmospheric circulation trends. *Journal of Climate*, 13.**3**, 617–633.

Dickson, R., Osborn, T., Hurrell, J., Meincke, J., Blindheim, J., Adlandsvik, B., Vinje, T., Alekseev, G. & Maslowski, W. (2000): The Arctic ocean response to the North Atlantic oscillation. *Journal of Climate*, 13.**15**, 2671–2696.

Drews, A., Greatbatch, R. J., Ding, H., Latif, M. & Park, W. (2015): The use of a flow field correction technique for alleviating the North Atlantic cold bias with application to the Kiel Climate Model. *Ocean Dynamics*, 65.**8**, 1079–1093.

Fang, Z. & Wallace, J. M. (1994): Arctic sea ice variability on a timescale of weeks and its relation to atmospheric forcing. *Journal of Climate*, 7.**12**, 1897–1914.

Flato, G., Marotzke, J., Abiodun, B., Braconnot, P., Chou, S. C., Collins, W. J., Cox, P., Driouech, F., Emori, S., Eyring, V. et al., (2013): Evaluation of Climate Models. In: Climate Change 2013: The Physical Science Basis. Contribution of Working Group I to the Fifth Assessment Report of the Intergovernmental Panel on Climate Change. *Climate Change 2013*, 5, 741–866.

Francis, J. A. & Vavrus, S. J. (2012): Evidence linking Arctic amplification to extreme weather in mid-latitudes. *Geophysical Research Letters*, 39.**6**, 1–6.

Frankignoul, C., Sennéchael, N. & Cauchy, P. (2014): Observed Atmospheric Response to Cold Season Sea Ice Variability in the Arctic. *Journal of Climate*, 27.**3**, 1243–1254.

Hurrell, J. W. (1995): Decadal trends in the North Atlantic Oscillation: regional temperatures and precipitation. *Science*, 269.**5224**, 676–679.

– (1996): Influence of variations in extratropical wintertime teleconnections on Northern Hemisphere temperature. *Geophysical Research Letters*, 23.**6**, 665–668.

Jolliffe, I. T. (2002): Principal Component Analysis. *Springer Series in Statistics*, 1–6.

Keeley, S. P. E., Sutton, R. T. & Shaffrey, L. C. (2012): The impact of North Atlantic sea surface temperature errors on the simulation of North Atlantic European region climate. *Quarterly Journal of the Royal Meteorological Society*, 138.**668**, 1774–1783.

Knight, J. R., Allan, R. J., Folland, C. K., Vellinga, M. & Mann, M. E. (2005): A signature of persistent natural thermohaline circulation cycles in observed climate. *Geophysical Research Letters*, 32.**20**.

Kwok, R., Cunningham, G., Wensnahan, M., Rigor, I., Zwally, H. & Yi, D. (2009): Thinning and volume loss of the Arctic Ocean sea ice cover: 2003-2008. *Journal of Geophysical Research: Oceans*, 114.**C7**.

Kwok, R. (2000): Recent changes in Arctic Ocean sea ice motion associated with the North Atlantic Oscillation. *Geophysical Research Letters*, 27.**6**, 775–778.

Lazier, J. R. N. (1994): Observations in the Northwest Corner of the North Atlantic Current. *Journal of Physical Oceanography*, 24.**7**, 1449–1463.

Madec, G. (2015): Nemo ocean engine. *Note du Pole de modélisation*, **27**, 5–300.

Mahajan, S., Zhang, R. & Delworth, T. L. (2011): Impact of the Atlantic Meridional Overturning Circulation (AMOC) on Arctic Surface Air Temperature and Sea Ice Variability. *Journal of Climate*, 24.**24**, 6573–6581.

Park, T., Park, W. & Latif, M. (2016): Correcting North Atlantic sea surface salinity biases in the Kiel Climate Model: influences on ocean circulation and Atlantic Multidecadal Variability. *Climate Dynamics*, 1–18.

Park, W., Keenlyside, N., Latif, M., Ströh, A., Redler, R., Roeckner, E. & Madec, G. (2009): Tropical Pacific climate and its response to global warming in the Kiel Climate Model. *Journal of Climate*, 22.**1**, 71–92.

Partington, K., Flynn, T., Lamb, D., Bertoia, C. & Dedrick, K. (2003): Late twentieth century Northern Hemisphere sea-ice record from US National Ice Center ice charts. *Journal of Geophysical Research: Oceans*, 108.**C11**.

Pedersen, R. A., Cvijanovic, I., Langen, P. L. & Vinther, B. M. (2016): The Impact of Regional Arctic Sea Ice Loss on Atmospheric Circulation and the NAO. *Journal of Climate*, 29.**2**, 889–902.

Petrie, R. E., Shaffrey, L. C. & Sutton, R. T. (2015): Atmospheric Impact of Arctic Sea Ice Loss in a Coupled Ocean–Atmosphere Simulation. *Journal of Climate*, 28.**24**, 9606–9622.

Polyakov, I. V., Alexeev, V. A., Bhatt, U. S., Polyakova, E. I. & Zhang, X. (2010): North Atlantic warming: patterns of long-term trend and multidecadal variability. *Climate Dynamics*, 34.**2-3**, 439–457.

Reintges, A., Latif, M. & Park, W. (2016): Sub-decadal North Atlantic Oscillation variability in observations and the Kiel Climate Model. *Climate Dynamics*, 1–13.

Roeckner, E., Bäuml, G., Bonaventura, L., Brokopf, R., Esch, M., Giorgetta, M., Hagemann, S., Kirchner, I., Kornblueh, L., Manzini, E. et al., (2003): The atmospheric general circulation model ECHAM 5. PART I: Model description. *Max Planck Institute for Meteorology Report*, **349**, 5–119.

Semenov, V. A., Latif, M., Dommenget, D., Keenlyside, N. S., Strehz, A., Martin, T. & Park, W. (2010): The Impact of North Atlantic–Arctic Multidecadal Variability on Northern Hemisphere Surface Air Temperature. *Journal of Climate*, 23.**21**, 5668–5677.

Semenov, V. A., Latif, M., Jungclaus, J. H. & Park, W. (2008): Is the observed NAO variability during the instrumental record unusual? *Geophysical Research Letters*, 35.**11**.

Semenov, V. A., Park, W. & Latif, M. (2009): Barents Sea inflow shutdown: A new mechanism for rapid climate changes. *Geophysical Research Letters*, 36.**14**.

Singarayer, J. S. & Bamber, J. L. (2003): EOF analysis of three records of sea-ice concentration spanning the last 30 years. *Geophysical research letters*, 30.**5**.

Skeie, P. (2000): Meridional flow variability over the Nordic seas in the Arctic Oscillation framework. *Geophysical research letters*, 27.**16**, 2569–2572.

Smedsrud, L. H., Esau, I., Ingvaldsen, R. B., Eldevik, T., Haugan, P. M., Li, C., Lien, V. S., Olsen, A., Omar, A. M., Otterå, O. H. et al., (2013): The role of the Barents Sea in the Arctic climate system. *Reviews of Geophysics*, 51.**3**, 415–449.

Stroeve, J., Holland, M. M., Meier, W., Scambos, T. & Serreze, M. (2007): Arctic sea ice decline: Faster than forecast. *Geophysical research letters*, 34.**9**.

Stroeve, J., Serreze, M. C., Holland, M. M., Kay, J. E., Malanik, J. & Barrett, A. P. (2012): The Arctic's rapidly shrinking sea ice cover: a research synthesis. *Climatic Change*, 110.**3-4**, 1005–1027.

Thompson, D. W. J. & Wallace, J. M. (1998): The Arctic oscillation signature in the wintertime geopotential height and temperature fields. *Geophysical Research Letters*, 25.**9**, 1297–1300.

Valcke, S. (2013): The oasis3 coupler: a european climate modelling community software. *Geoscientific Model Development*, **6**, 373–388.

van der Swaluw, E., Drijfhout, S. S. & Hazeleger, W. (2007): Bjerknes Compensation at High Northern Latitudes: The Ocean Forcing the Atmosphere. *Journal of Climate*, 20.**24**, 6023–6032.

Vaughan, D. G., Comiso, J. C., Allison, I., Carrasco, J., Kaser, G., Kwok, R., Mote, P., Murray, T., Paul, F., Ren, J. et al., (2013): Observations: cryosphere. *Climate change*, 317–382.

Vihma, T. (2014): Effects of Arctic sea ice decline on weather and climate: a review. *Surveys in Geophysics*, 35.**5**, 1175–1214.

von Storch, H. & Zwiers, F. W. (1999): Statistical Analysis in Climate Research. *Cambridge university press*, 291–296.

Wallace, J. M. & Thompson, D. W. J. (2002): The Pacific Center of Action of the Northern Hemisphere Annular Mode: Real or Artifact? *Journal of Climate*, 15.**14**, 1987–1991.

Wang, C., Zhang, L., Lee, S.-K., Wu, L. & Mechoso, C. R. (2014): A global perspective on CMIP5 climate model biases. *Nature Climate Change*, 4.**3**, 201–205.

Yeh, S.-W., Kirtman, B. P., Kug, J.-S., Park, W. & Latif, M. (2011): Natural variability of the central Pacific El Niño event on multi-centennial timescales. *Geophysical Research Letters*, 38.**2**, 1–2.

Appendix

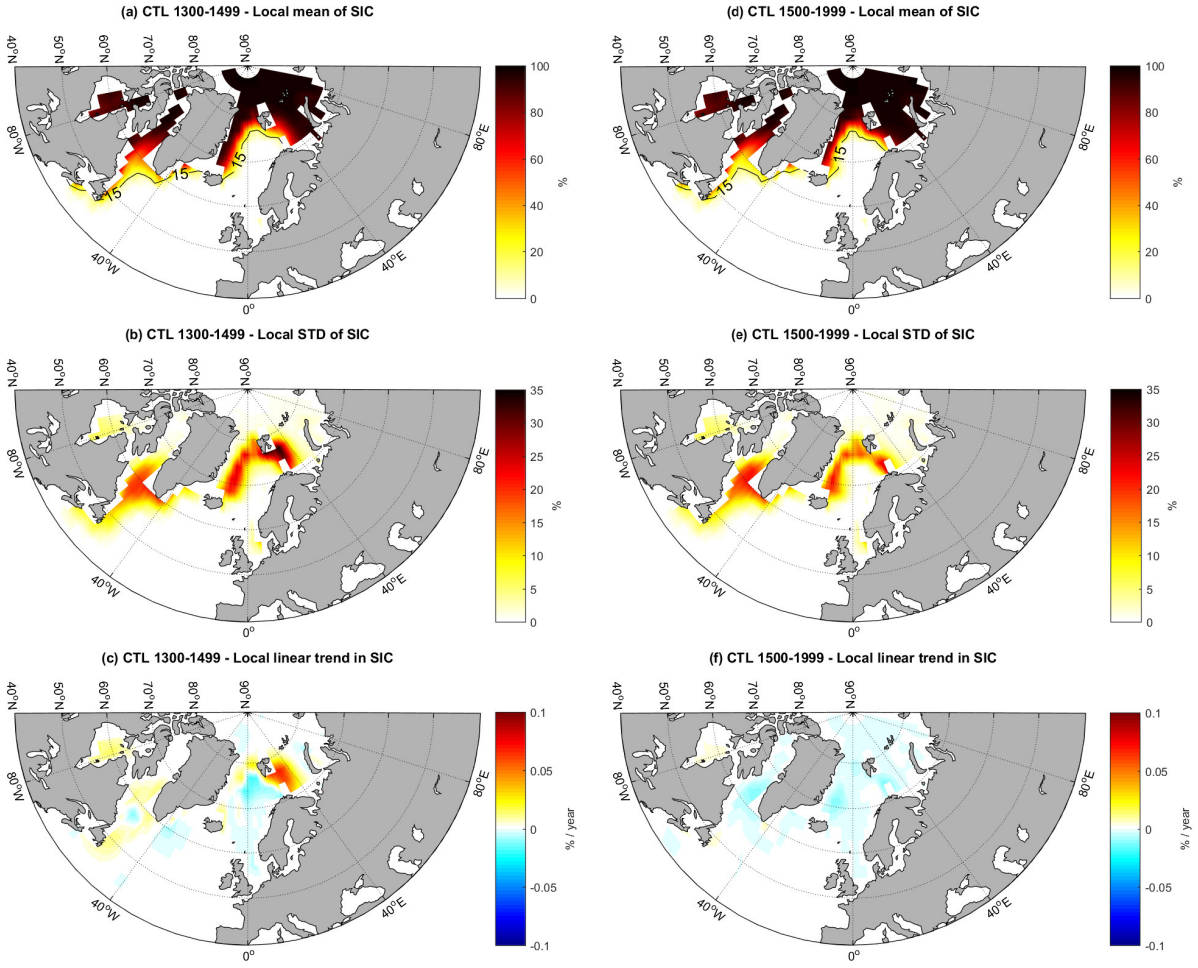

Fig. 13: Local mean and local STD of sea ice concentration for CTL's first period (1300-1499) are shown (a, b). CTL's second period (1500-1999) mean and STD of sea ice concentration are depicted (d, e). The local linear trends for both period are shown (c, f). The 15 % edge for sea ice is marked with a black line in (a) and (b).

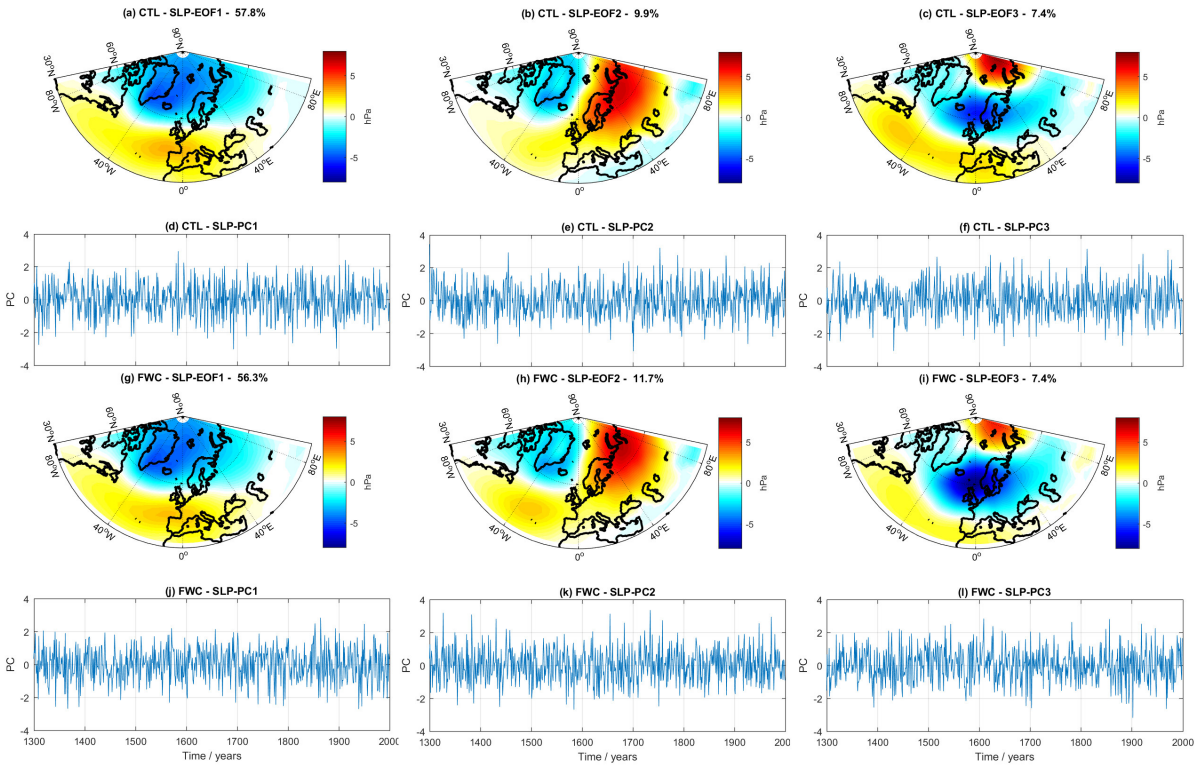

Fig. 14: The three leading modes of wintertime SLP anomalies for the Atlantic sector of the Northern Hemisphere are shown for CTL (a-c). The corresponding PCs can be seen in (d-f). The respective EOF patterns and PCs for FWC are shown (g-l).

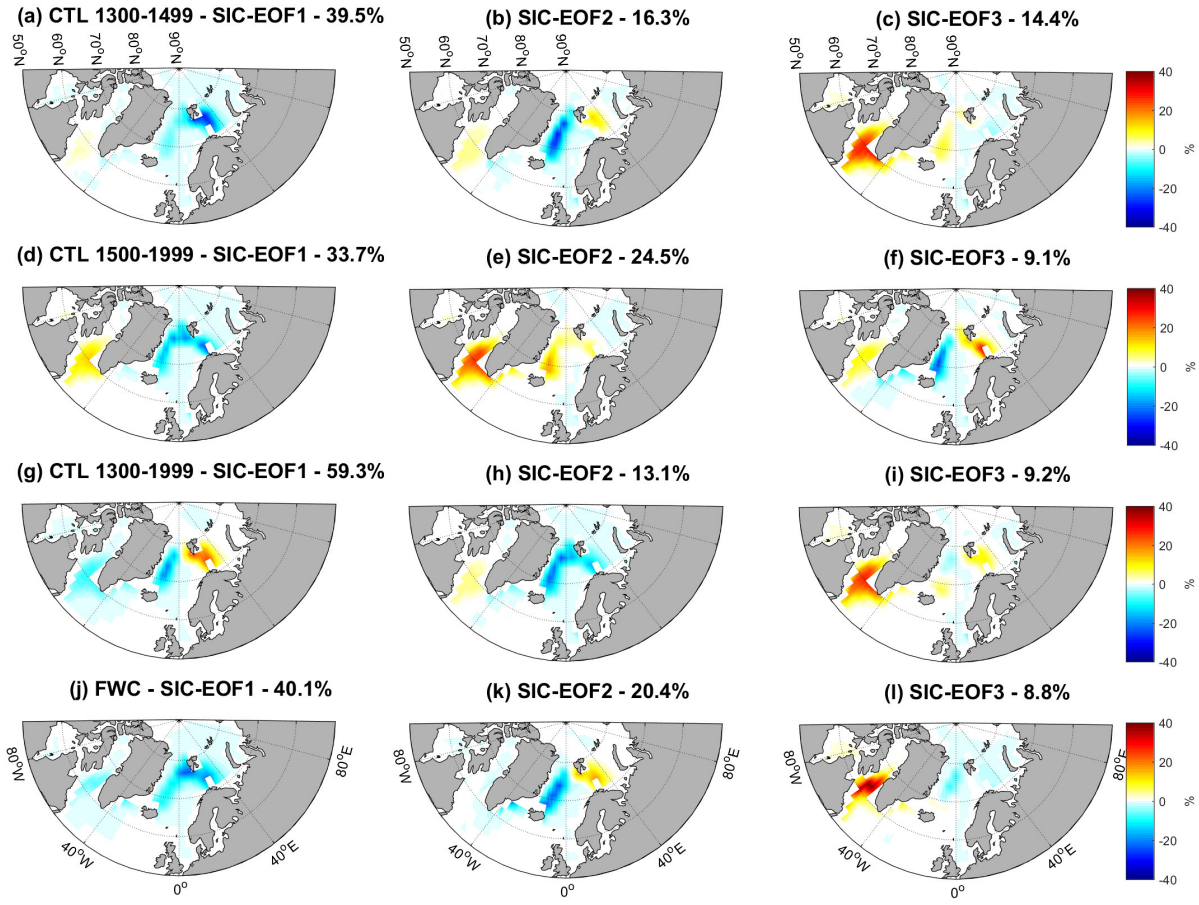

Fig. 15: EOF1-3 for CTL's first period (1300-1499) (a-c), second period (1500-1999) (d-f), full period (g-i) and for FWC (j-l) are shown.

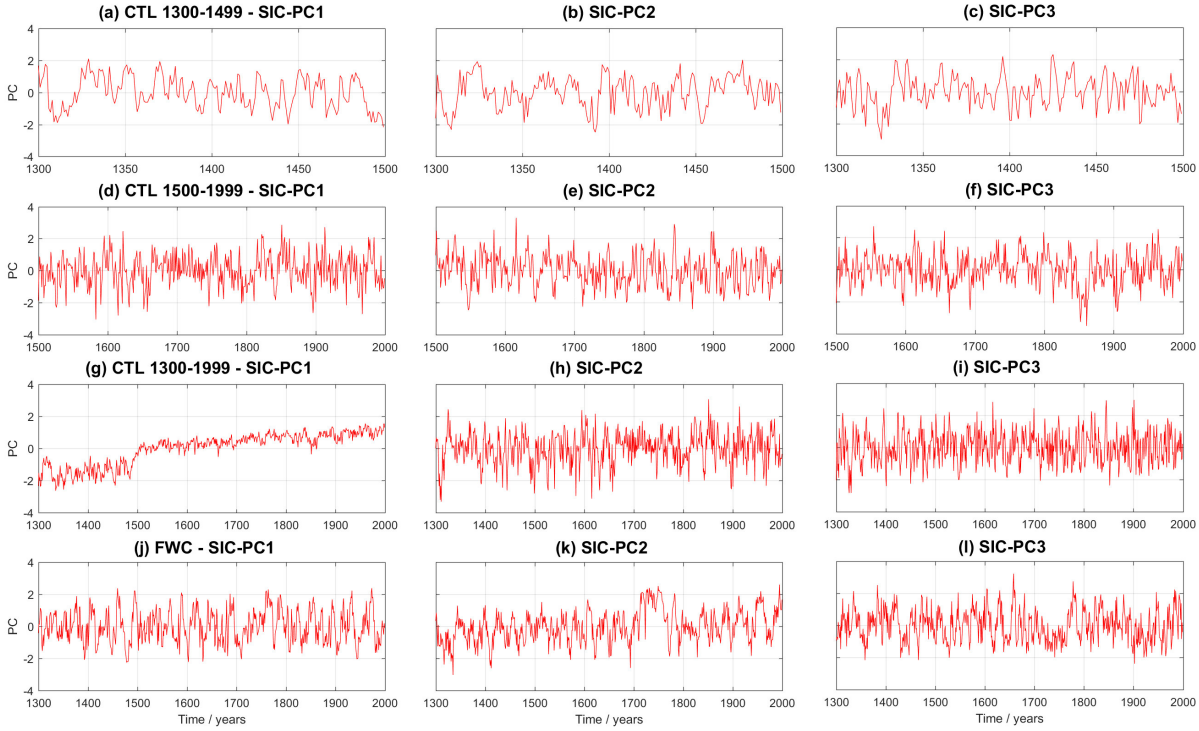

Fig. 16: PC1-3 for CTL's first period (1300-1499) (a-c), second period (1500-1999) (d-f), full period (g-i) and for FWC (j-l) are shown.

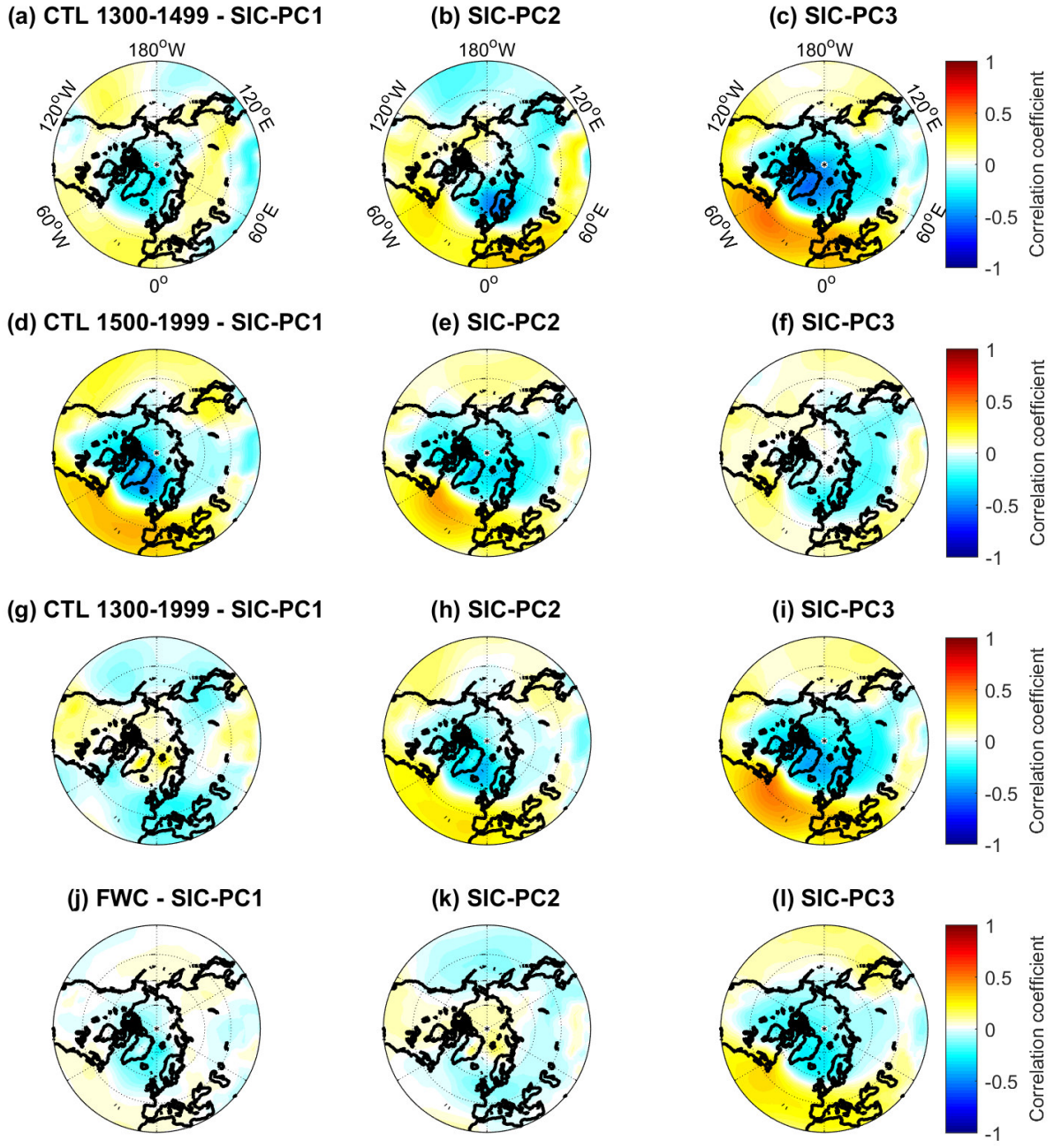

Fig. 17: Correlations of SIC-PC1-3 with local SLP for CTL's first period (1300-1499) (a-c), second period (1500-1999) (d-f), full period (g-i) and for FWC (j-l) are shown.

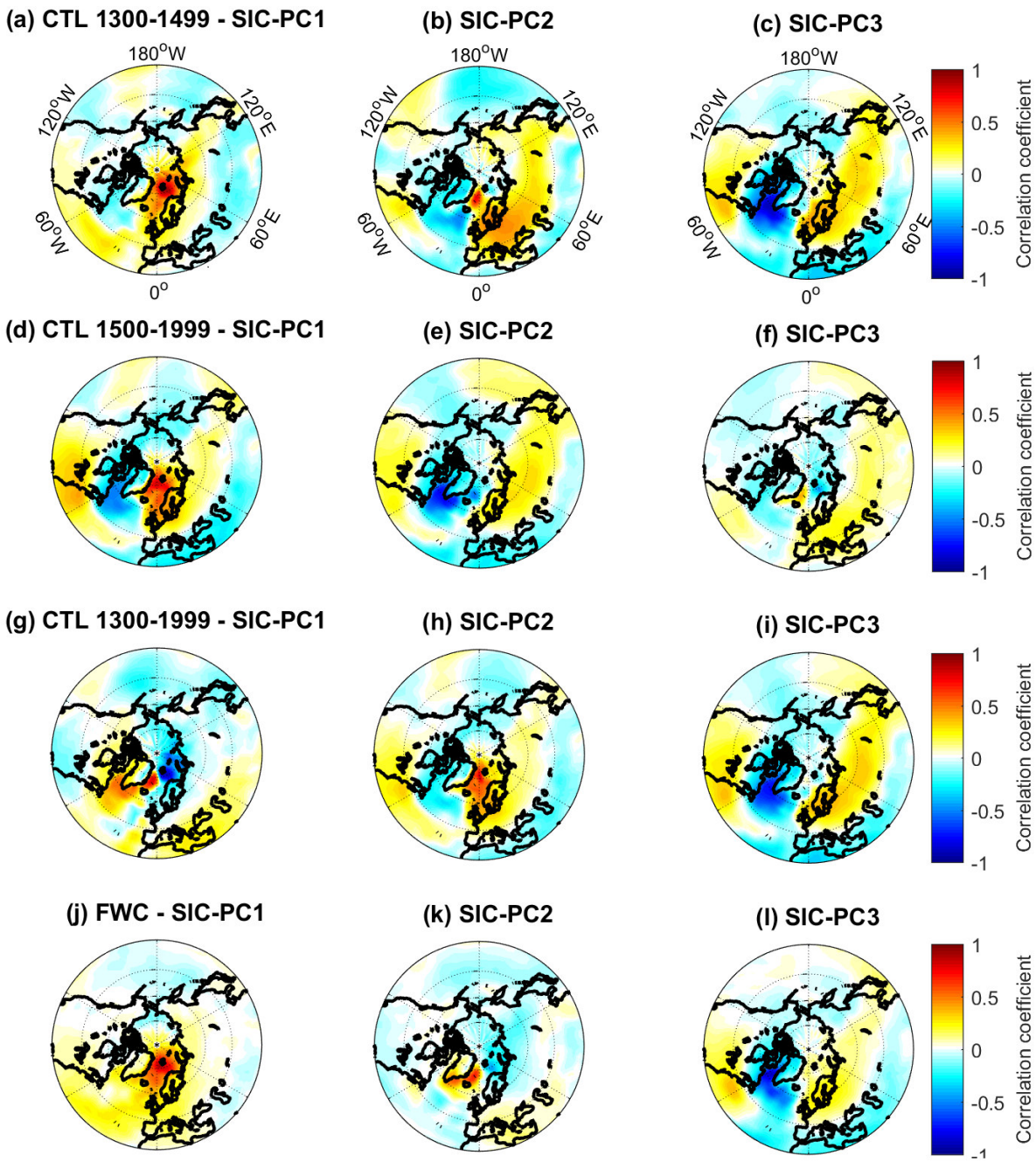

Fig. 18: Correlations of SIC-PC1-3 with local SAT for CTL's first period (1300-1499) (a-c), second period (1500-1999) (d-f), full period (g-i) and for FWC (j-l) are shown.

Erklärung

Hiermit erkläre ich, Philip Kreußler, dass ich die Bachelorarbeit selbstständig und nur mit Hilfe der angegebenen Referenzen und Hilfsmittel angefertigt habe.
Die eingereichte schriftliche Version stimmt mit der auf dem elektronischen Speichermedium überein.
Weiter bestätige ich, dass ich diese Arbeit noch nicht für einen Abschluss an anderer Stelle eingereicht habe.

Kiel, den 17. Oktober 2016 — Philip Kreußler